SPACE-TIME STRUCTURE OF CHANGES IN ATMOSPHERIC ANGULAR MOMENTUM

BY

John Roberts Anderson
S.B., Massachusetts Institute of Technology (1976)

Submitted to the Department of Meteorology
and Physical Oceanography in partial
fulfillment of the degree of

Master of Science

at the
Massachusetts Institute of Technology

May 1982

Signature of Author _____
Department of Meteorology
and Physical Oceanography
May, 1982

Certified by _____
Reginald E. Newell
Thesis Supervisor

Accepted by _____
Ronald G. Prinn
Chairman, Departmental Committee
on Graduate Students

SPACE-TIME STRUCTURE OF CHANGES IN ATMOSPHERIC ANGULAR MOMENTUM

by

JOHN ROBERTS ANDERSON

Submitted to the Department of Meteorology and Physical Oceanography on May 7, 1982 in partial fulfillment of the requirements for the degree of Master of Science in Meteorology

ABSTRACT

The variations in total relative angular momentum of the atmosphere are examined for annual and shorter time scales. Use of a 5 year data set consisting of zonally-averaged values from the NMC twice daily analysis allows the construction of 2-dimensional (latitude-height) descriptions of the phenomena.

Spatially coherent patterns have been identified associated with annual, semi-annual, and 40-50 day periods. An empirical orthogonal function (EOF) analysis provides a good spatial description of structures with primarily annual and semi-annual variations. These structures are very similar to those described by Newell et al. (1974) based on a Fourier decomposition of the zonal wind field. To describe the 40-50 day variations, an amplitude-phase extension of the EOF technique was used. This 'oscillation' consists of a tropical component which is similar to the motions described by Madden and Julian (1971, 1972), and a coherently connected northern hemisphere mid-latitude component which is believed to be previously unreported. The tropical component shows well-defined phase propagation downward and poleward, while the northern hemisphere 'teleconnection' has phase essentially independent of height.

Thesis Supervisor: Dr. Reginald E. Newell

Title: Professor of Meteorology

TABLE OF CONTENTS

INTRODUCTION

The total relative atmospheric angular momentum, M, given by [1] is a quantity which has historically been more of theoretical interest to meteorologists as a dynamical constraint than as an object of observational interest, particularly on time scales shorter than one year.

$$M = \frac{a^3}{g} \int_{p_s}^{0} \int_{0}^{2\pi} \int_{-\pi/2}^{\pi/2} U \cos^2\varphi \, d\varphi \, d\lambda \, dp \qquad [1]$$

Where U = zonal wind,
φ = latitude,
λ = longitude,
p = pressure,
a = earth radius,
g = gravitational acceleration,
and p_s = surface pressure.
This equation is derived for a thin (scale height $\ll$ a) hydrostatic atmosphere.

Recently there has been increased interest in this quantity primarily because of its' relationship to the earth's rotation rate or length of day (LOD). The only significant torques acting on the total earth-atmosphere system are gravitational tides. These tidal forces primarily introduce periodic monthly and semi-monthly changes and a slow, rather steady increase in length of day.

Some changes in the length of day may be due to geophysical effects such as large spatial scale earthquakes and core-mantle coupling; however these effects are believed, somewhat empirically, to be weaker than meteorological effects on time scales from tens of days to one year (Hide et al.

1980, Langley et al., 1981). On this time scale it would then seem reasonable to treat the total angular momentum of the system as a conserved quantity, with possible corrections for monthly and semi-monthly tides, and associate all changes in LOD with transfers of M between the atmosphere and the solid earth through surface friction and form drag (mountain torque) terms. This assumption yields a relationship between changes in M and changes in LOD given by [2].

$$\frac{\Delta LOD}{LOD} = \frac{\Delta M}{I_s} \frac{1}{\omega} \qquad [2]$$

Where Δ represents the change in a quantity from some mean value, I_s = moment of inertia, and ω = the rotation angular frequency of the earth.

I_s in this equation represents the moment of inertia, about the rotation axis, of the part of the planet which participates in these changes. This is generally taken to be the crust and mantle with a decoupled core. A value for I_s computed from a seismologically inferred density model is $7.04 \cdot 10^{37}$ KgM^2 (Jordan et al., 1974) yielding a linear relationship , [3], between M and LOD (Langley et al., 1981).

$$\Delta LOD = 1.68 \cdot 10^{-29} \Delta M \qquad [3]$$

ΔLOD in S, ΔM in KgM^2S^{-1}

This relationship is of interest in a meteorological context because LOD is a quantity which can now be measured

with great accuracy independently of any meteorological input (Lambeck 1980). An example of such a time series is given in the next section. It will become apparent in the following sections that the M time series is a surprisingly good indicator of coherent atmospheric motions with annual, semi-annual, and 40-50 day time scales. This perhaps purely fortuitous relationship allows an independent estimate of the magnitude of, and in the case of the 40-50 day 'oscillation' the reality of these effects. This is particularly important because the only easily analyzed daily M records start with January 1976, while LOD records with 5 day resolution from lunar laser ranging and other techniques exist back to at least 1971 (Langley et al., 1981).

Descriptions of the data analyses which have been performed are divided into four sections. The first describes the data sets and techniques used in the estimation of M. In the second the seasonal variations are examined. In the third, non-seasonal anomaly values are computed, and various forms of spectral analysis and filtering techniques are employed for guidance in finding the spatial structure of the changes. The fourth section examines the space-time structure of the non-seasonal changes, particularly the 40-50 day 'oscillation'.

Due to the short length of the data set (5 years) no attempt has been made to examine variations on a time scale longer than one year. It should be noted that the anomaly

time series exhibits significant low frequency power and work by Arkin (1981) and Selkirk (1982) indicates that 200 mb zonal winds are strongly correlated with the Southern Oscillation Index in a way that would indicate a contribution to the atmospheric angular momentum. Future studies could probably gainfully apply techniques similar to those used in this work to fields of low pass filtered monthly-mean winds to describe the low frequency variations.

THE MEASUREMENT OF ATMOSPHERIC RELATIVE ANGULAR MOMENTUM

The principal data set used in this work was constructed from the National Meteorological Center (NMC) twice daily (0Z, 12Z) analyses. The data set represents values of the zonally averaged zonal winds, [U], at 73 latitudes (2.5° spacing) and 12 pressure levels (1000, 850, 700, 500, 400, 300, 250, 200, 150, 100, 70, and 50 mb). The zonally averaged data are available for about 80% of the period with the largest gaps on the order of 4 days. On many days only the 0Z values are available. A more complete description of the data set is given by Rosen and Salstein (1981). It should be emphasized that without the existence of the precomputed zonal averages, the compilation of an M time series from the NMC analyses would have been computationally awesome. This is the primary reason for the unavailability of data for periods before 1976.

The NMC final analysis includes data from radiosonde,

aircraft and satellite sources. The use of this data set for general circulation studies has been examined by Lau et al., (1981) and Rosen and Salstein (1980). In these papers the authors compared various quantities computed from the NMC analysis and another data set computed from station observations using an objective analysis scheme. The degree of correlation varied, particularly for derived quantities such as fluxes. However U appeared to be a relatively robust quantity with analysis-produced variations in $\overline{[U]}$ being less than 10% of its mean value. It sould be noted that the NMC analysis scheme makes use of a numerical model forecast as the initial guess and there is a possibility that variations in the output fields, particularly in data sparse regions, may represent the model's rather than the atmosphere's physics. This problem should be severe only for very short time scale motions, on the order of a few days, and the presence of the feature in the independently measured LOD time series will serve to alleviate these fears.

The first step in the data analysis was the construction of a daily data set for all latitudes and the lowest 10 levels. The 70 and 50 mb data were not used due to concern about their accuracy (Rosen and Salstein, 1981). The OZ and 12Z values were averaged when both were available; if neither was available the missing datum was linearly interpolated between existing daily values. The NMC southern hemisphere data for 1976 contains a large step-like change of dubious

reality which is examined in Appendix A. For this reason data before this event have not been included in the computation of any statistics although they appear on the plots of time series.

The 1977-1980 means for [U] are shown in Figure 2-1. These values of $\overline{[U]}$ agree well (~10% variation) with measurements of other time periods using station data (Newell et al., 1972 Starr et al., 1970). Figure 2-2 shows the standard deviation of [U] taken daily for the period. Note that the major peaks are equatorward of the northern and southern hemisphere jet cores and that the southern hemisphere jet shows significantly smaller variations although it has a larger mean velocity. These factors are in good agreement with the 12 month Fourier decomposition of zonal wind given by Newell et al. (1974) and shown in Figure 3-10.

Starting with the zonally averaged winds it is not possible to compute M as given in [1] because of the longitudinal variation of P_s. Instead an approximation of P_s = 1000 mb is made yielding [4].

$$M \sim \frac{2\pi a^2}{g} \int_{1000\,mb}^{0} \int_{-\pi/2}^{\pi/2} [U] \cos^2\varphi \, d\varphi \, dp \qquad [4]$$

Where [] is the traditional zonal average operator. This quantity is estimated from the data set by [5].

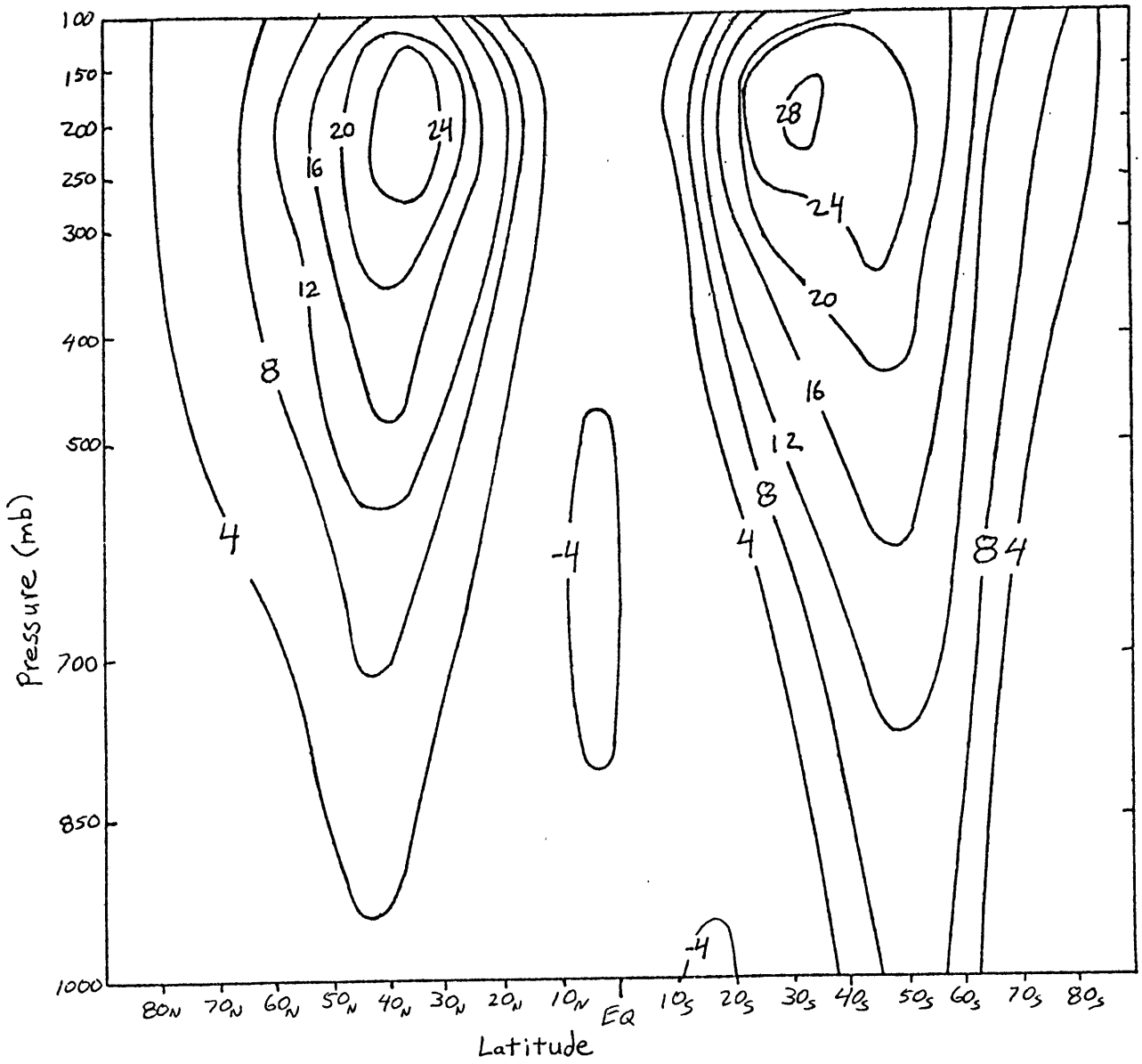

Fig. 2-1. Mean [U] (m/sec) 1977-1980

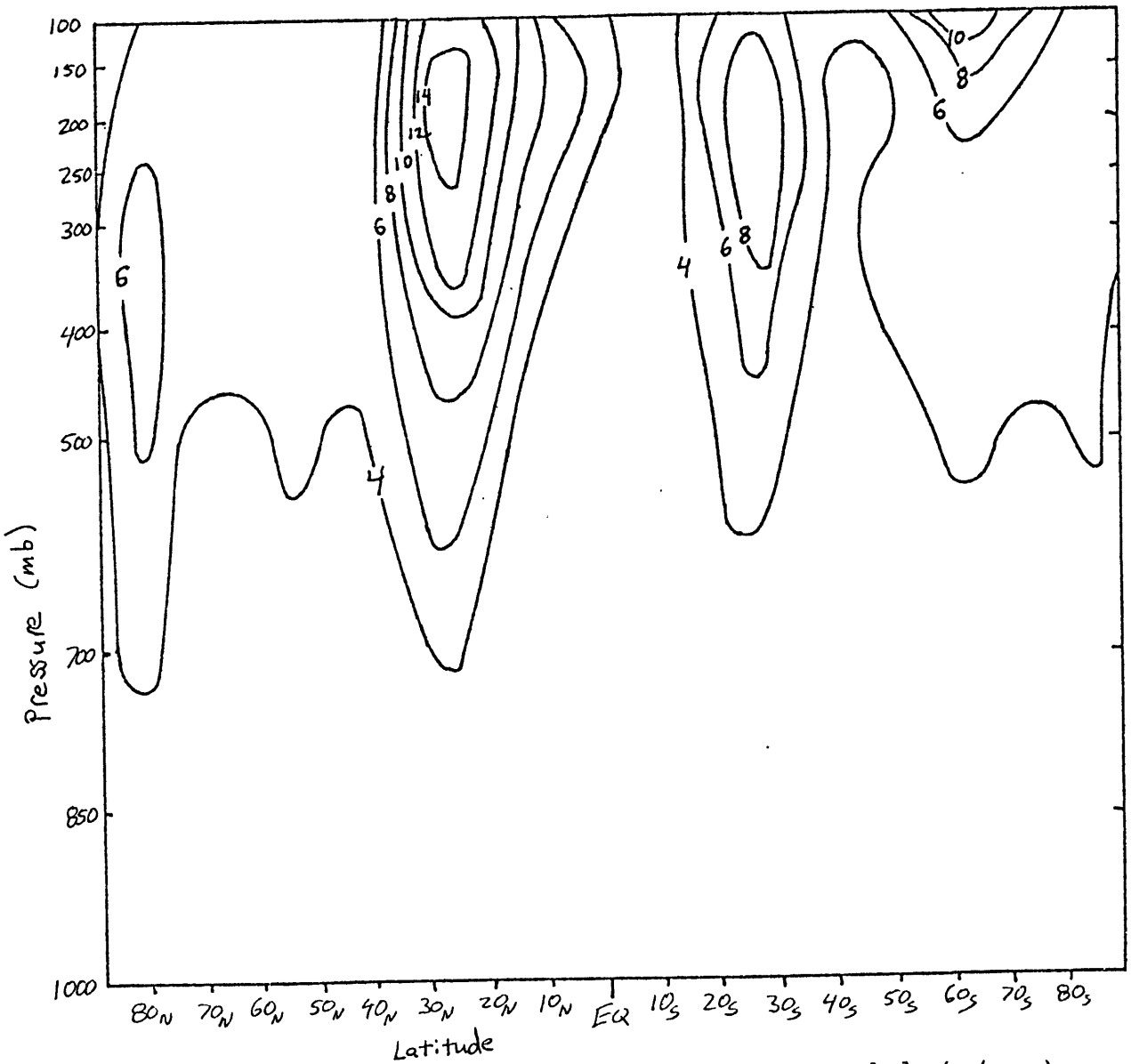

Fig. 2-2. Standard Deviation of daily [U] (m/sec)

$$M \sim \frac{2\pi a^3}{g} \sum_{P=1000mb}^{100mb} \nabla P(P) \sum_{\varphi=-87.5^\circ}^{87.5^\circ} [U](\varphi, P) \cos^2\varphi \qquad [5]$$

Where $\nabla P(P)$ is the thickness of a layer with central pressure P. $\nabla P(1000)$ is taken to be 75 mb (one-sided layer), and $\nabla P(100)$ is taken to be 50 mb so as to give equal weighting with the data for 250-150 mb.

The above weightings represent an approximation of [4] which includes contributions for 1000 to 75 mb using data from 1000 to 100 mb. As concluded by Rosen and Salstein (1981) it is very difficult to evaluate the error in such a computation; however, one would expect a possible bias of about 7.5% due to the omission of the top 75 mb.

A time series of daily atmospheric M values computed in this way for 1976-1980 is presented as Figure 2-3. This figure is essentially identical to the one computed from the same data set by Rosen and Salstein (1981). Figure 2-4 is a time series of the inferred value for M based on a 5-day resolution lunar laser ranging LOD record. The momentum scaling of the LOD series is in accordance with [3]. Notable features of these time series include a very strong yearly variation with an easily detectable semi-annual harmonic component. As discovered by Langley et al. (1981) there are 40-50 day period variations which show very good agreement between the two methods. The 40-50 day variations appear to occur asynchronously with the annual cycle.

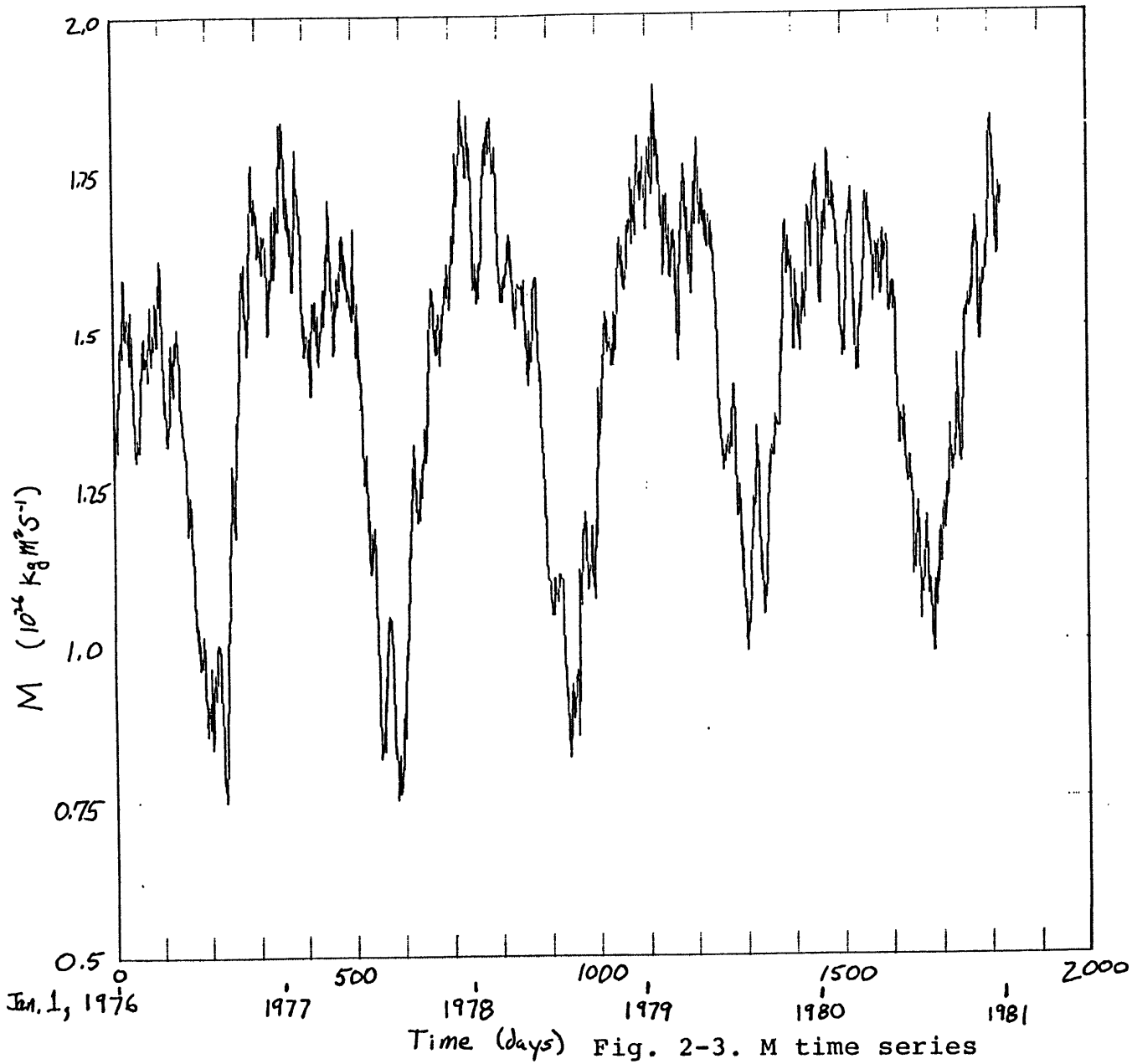

Fig. 2-3. M time series

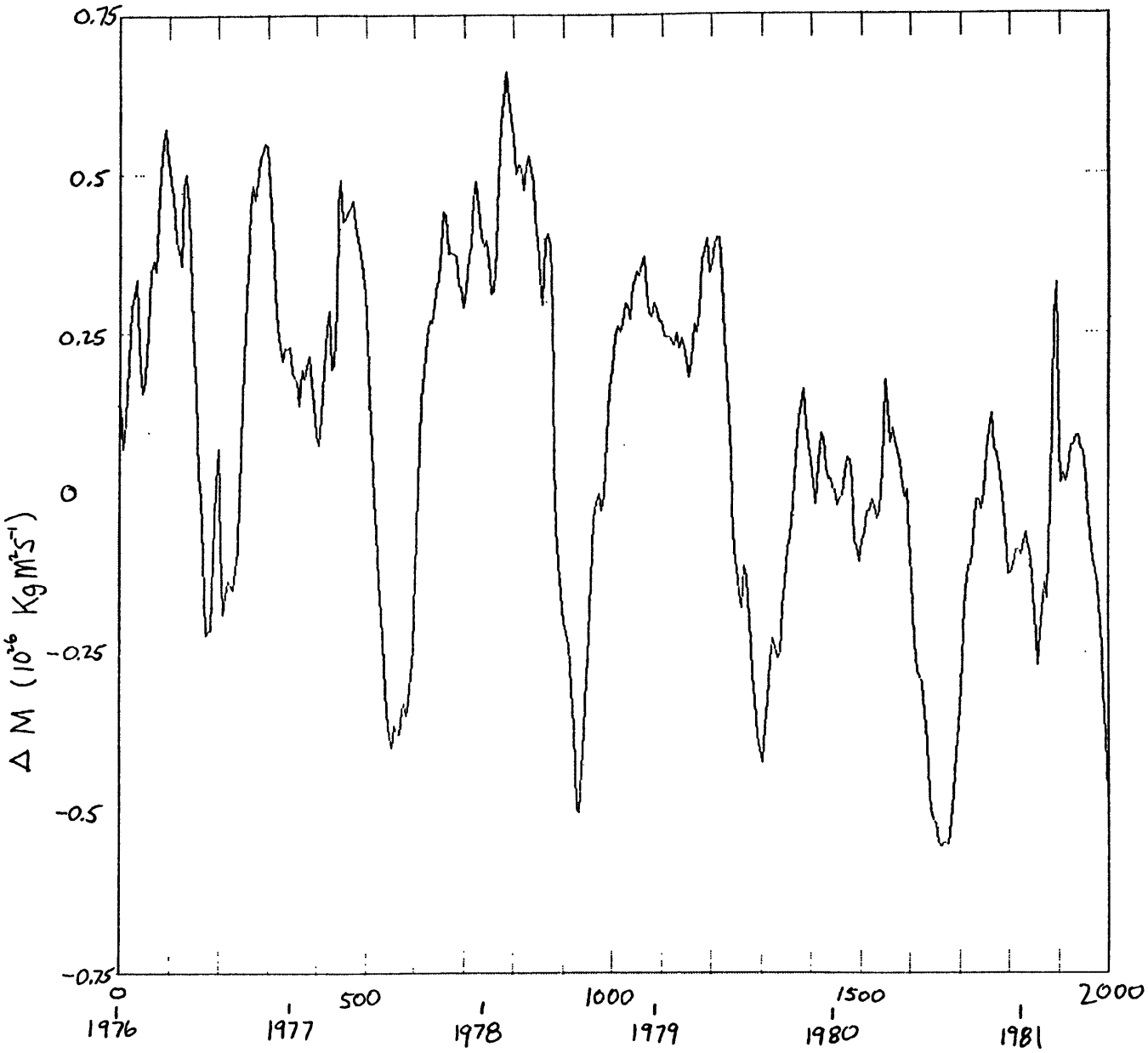

Fig. 2-4. M inferred from LOD, from Dr. R. Langley

One significant difference between the two measurements is the presence of a large low frequency variation in the LOD series. These variations are believed to possibly result from core-mantle interactions (Stacey 1981). It also appears that the LOD series exhibits a stronger semi-annual harmonic than the M series, this is entirely reasonable considering the structure of the semi-annual changes in [U] reported by Newell et al. (1974) and reproduced as Figure 3-10. This figure indicates the presence of important semi-annual contributions to M at altitudes above 100 mb. Another possible cause for the difference in the semi-annual amplitudes is the existence of annual and semi-annual solid body tides. A final comment on the comparison is that the LOD series does not appear to support the anomalously low values of M for early 1976 that are discussed in Appendix A.

THE STRUCTURE OF SEASONAL CHANGES

The next step in the examination of the data set was the construction of a seasonal cycle climatology for [U]. The year was divided into 92 4-day segments, the last containing only 1 day, 2 for leap years. The mean values for each latitude-pressure resolution cell were computed for each segment using the data from 1977-1980.

A plot of the mean annual cycle of M is given as Figure 3-1. The standard deviations of the [U]'s are shown in Figure 3-2.

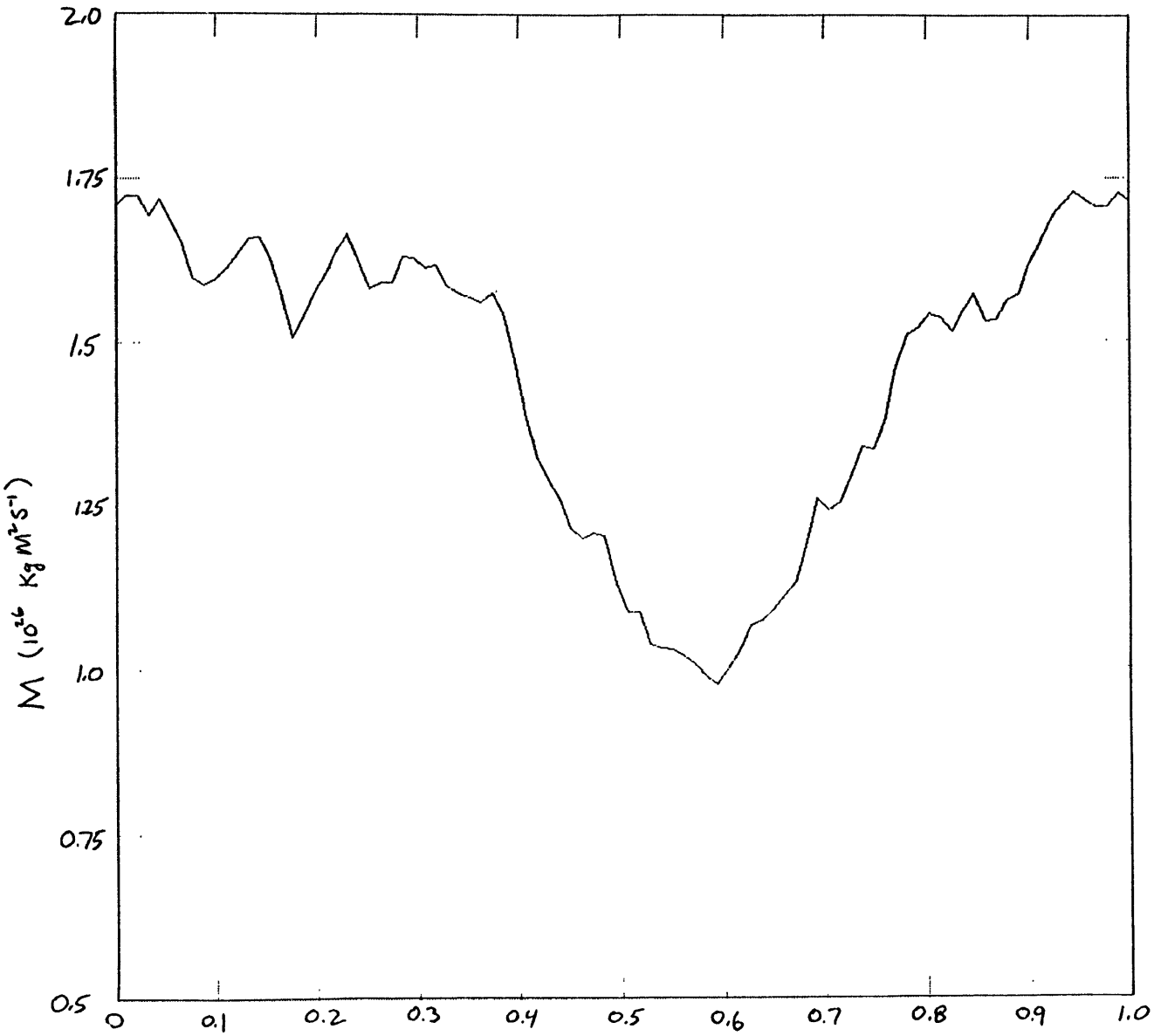

Fig. 3-1. Mean annual cycle of M

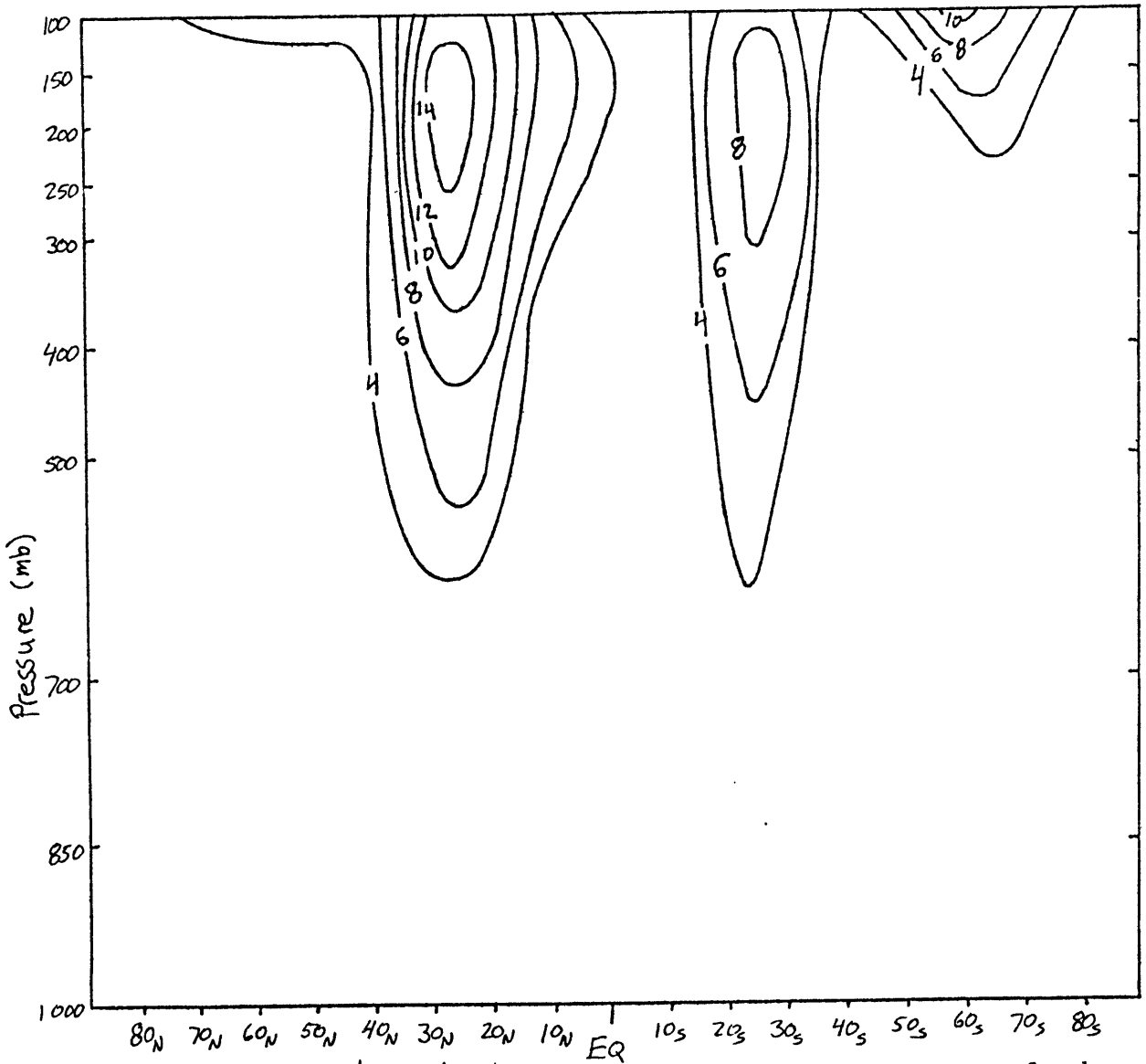

Fig. 3-2. Std. Dev. of seasonal changes (m/sec)

An analysis which has proven to be quite helpful in understanding the structure of the spatial patterns is the construction of a map consisting of correlation coefficients relating each latitude-pressure cell to a single time series. This produces a field depicting the square root of the fractional variance of that cell's [U] which is explained by the time series. Figure 3-3 is a contour plot of such a field for the seasonal climatological winds, where the time series was the M values derived from the same winds as the time series. The results of this analysis show the strong seasonal component in the regions of high standard deviation equatorward of the northern and southern hemisphere jets. The northern hemisphere jet is shown to be positively correlated with M and the southern negatively. The trade winds appear with the opposite sign consistent with increased easterlies in the winter hemisphere.

Empirical orthogonal function (EOF) analysis is a technique where a field of time series is expanded in the form given by [6].

$$\hat{[U]}^N(\varphi,p,t) = \sum_{n=1}^{N} a_n(\varphi,p)\, b_n(t) \qquad [6]$$

Where $\hat{[U]}^N$ is an order N estimate of [U].

It has been shown that for a given order N, the a's and b's which minimize a weighted error [7] are the eigenvectors of the weighted data covariance matrix corresponding

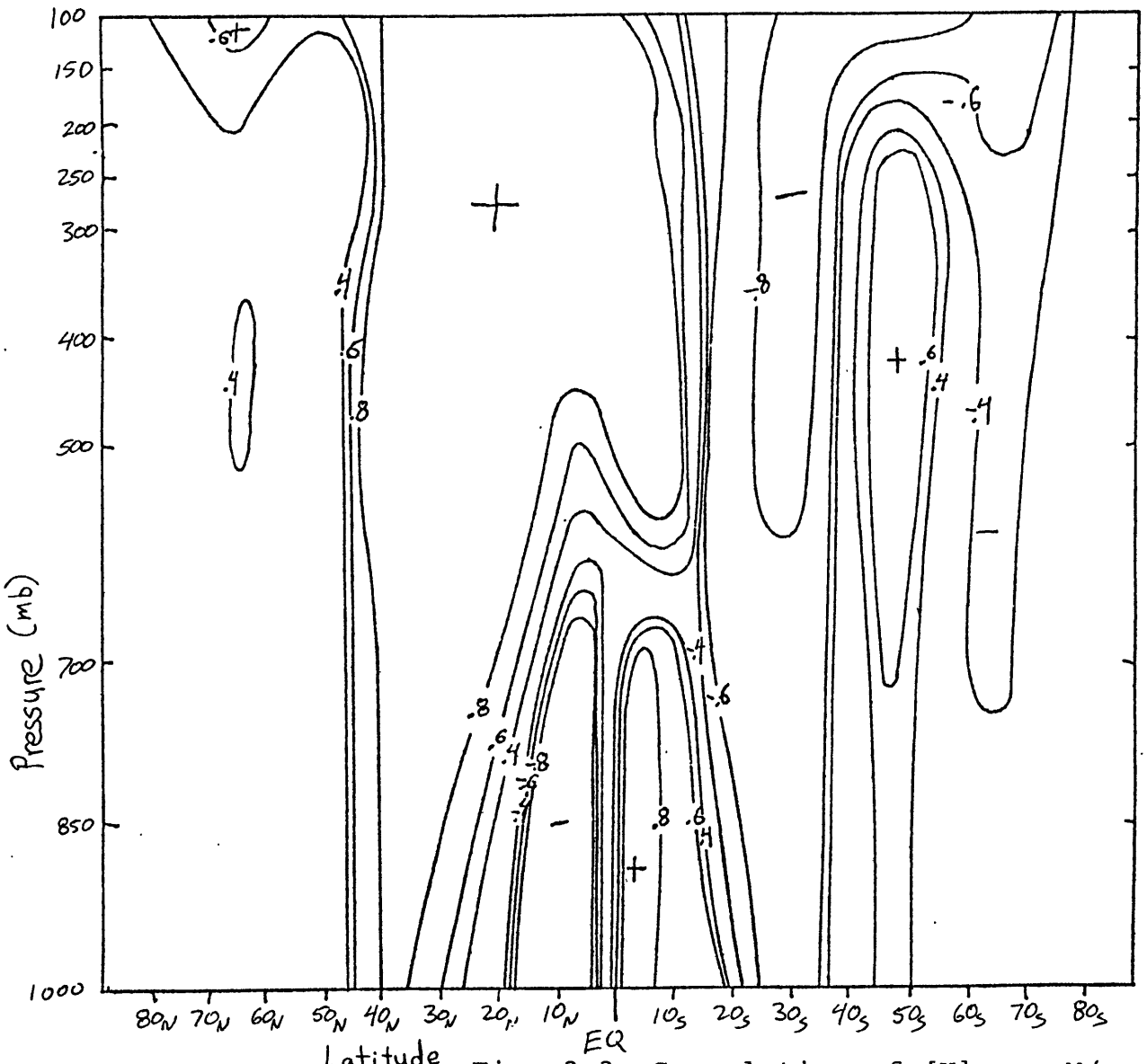

Fig. 3-3. Correlation of [U] vs. M(seasonal)

to the N largest eigenvalues (Lorenz 1957).

$$E_N^{-2} = \sum_{\varphi} W_{\varphi}(\varphi) \sum_{p} W_p(p) \sum_{t=1}^{M} \left([v](\varphi,p,t) - \hat{[v]}_N \right)^2 \qquad [7]$$

Where W_{φ}, and W_p are appropirate error weighting functions.

The a's are generally referred to as EOF's with the b's as associated time series. The hope, of course, is that the EOF's will separate the important physical processes represented in the data. This is not always the case and even under the best conditions the analysis cannot separate processes whose physics are not orthogonal.

The maximum number of independent eigenvectors which can be computed is equal to the number of spatial cells or the number of observations, whichever is less. It is possible to compute the eigenvectors corresponding to either the a's or b's depending on whether one constructs the covariance matrix to represent either the temporal or spatial variances respectively. In this work there are generally fewer independent observations, particularly with the filtered data set which is described in later sections, and I have chosen to compute the b's and find the a's from [8]. This method has been criticized by Rasmussen et al. (1981), who feel that it is subject to numerical inaccuracies and advocate finding ordered eigenvectors of the larger, singular covariance matrix. In spite of this concern I chose to find the eigenvectors of the smaller matrix as it is still by far

the easiest method to implement using available routines. For this data set, a test case produced EOF's that were indistinguishable.

$$a_n(\varphi, p) = \sum_t [U](\varphi, p, t)\, b_n(t) \qquad [8]$$

Where $b_n(t)$ has been normalized so that

$$\sum_t b_n^2(t) = 1$$

A measure of the effectiveness of a particular eigenvector is the fraction of the variance explained, which is equal to $(E_{N-1}^2 - E_N^2)/E_o^2$ where E_o^2 is the weighted sum of the squares of [U] (φ, p). The weighting functions have been taken to be $W_p = \nabla P(p)$ (see [5]), and $W_\varphi = \cos(\varphi)$. These values yield a mass weighted covariance matrix where E_N^2 is proportional to the zonal kinetic energy of the unexplained winds.

The first three EOF's of the seasonal changes explain 87.2%, 3.6%, and 3.5% of the variance. Contour plots of them are given as Figures 3-4 to 3-6. Figures 3-7 to 3-9 show correlation coefficient maps of the seasonal climatological [U] field vs. the time series of the EOF's. These plots, which are directly comparable to Figure 3-3, show where each EOF is effective in explaining the seasonal variation. The plots are proportional to a plot of the amplitude of the EOF

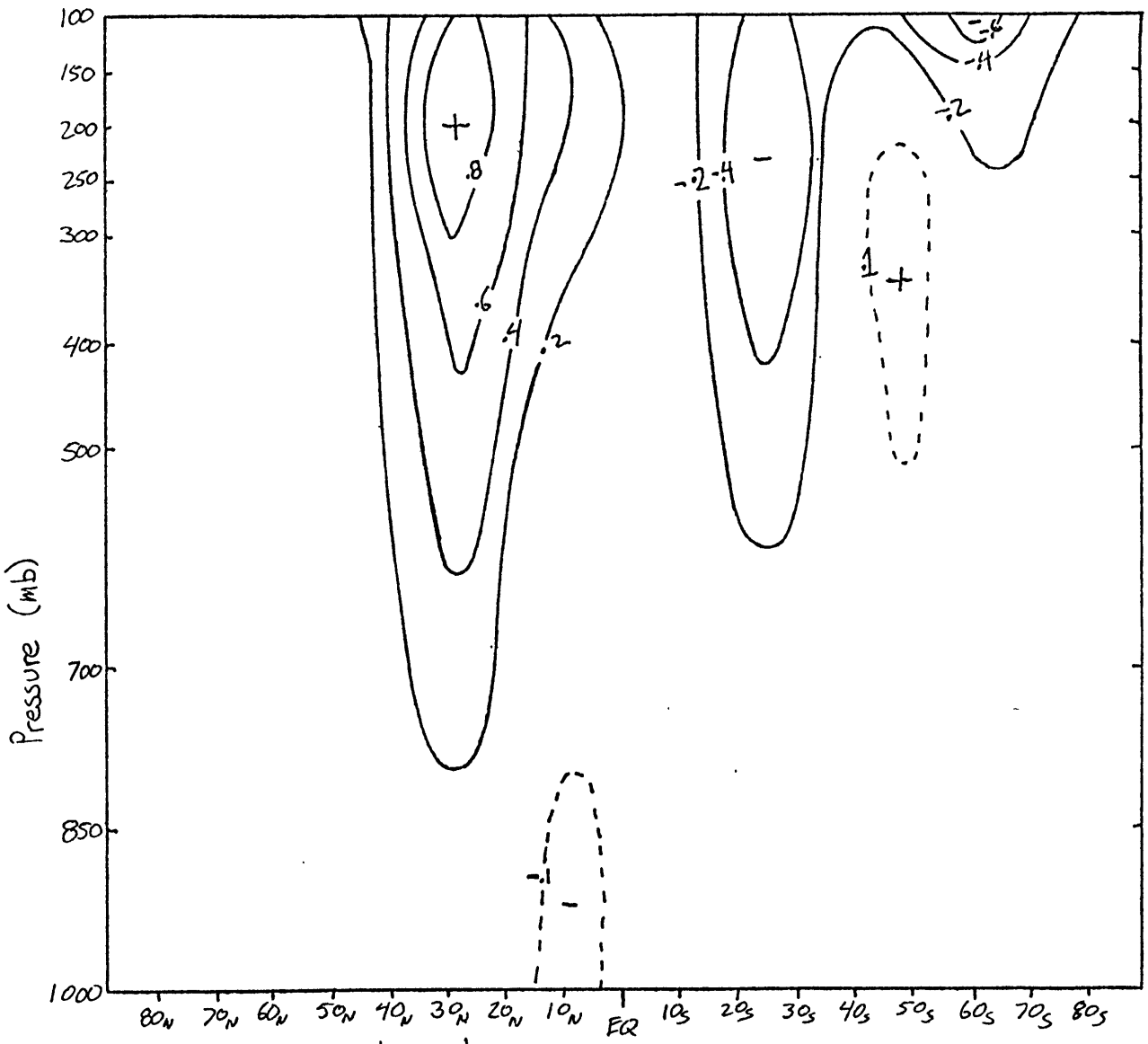

Fig. 3-4. Seasonal EOF 1

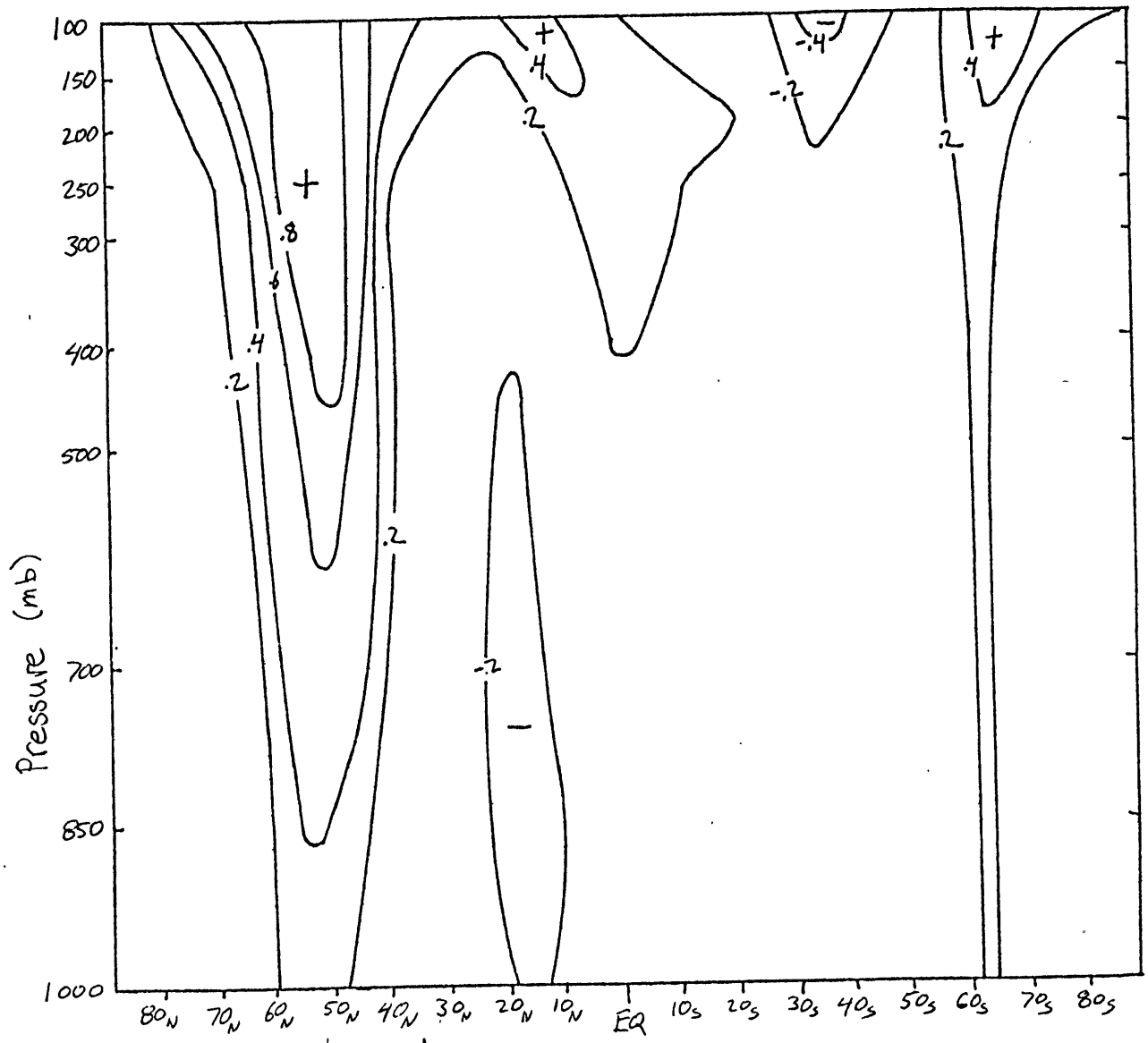

Fig. 3-5. Seasonal EOF 2

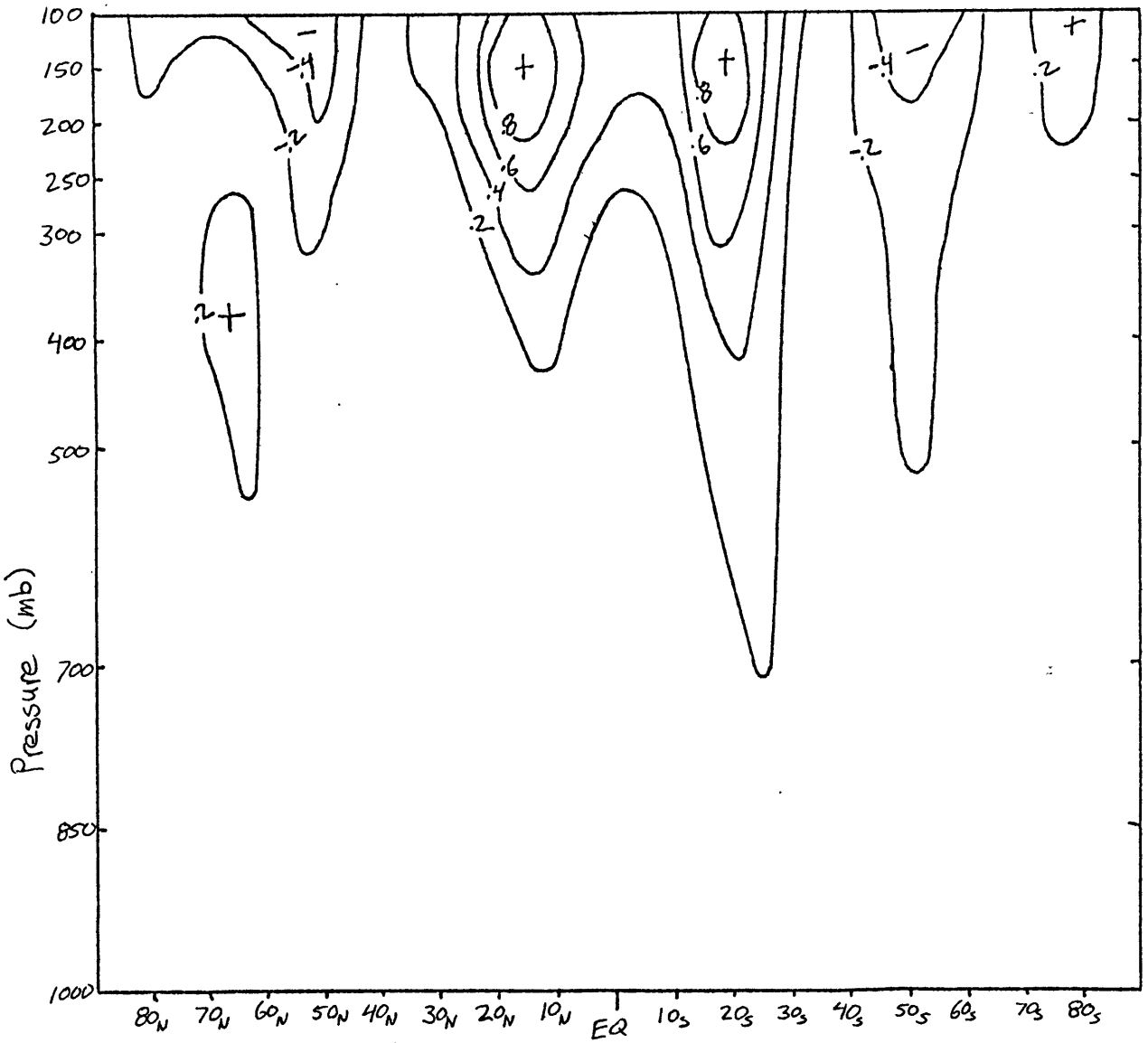

Fig. 3-6. Seasonal EOF 3

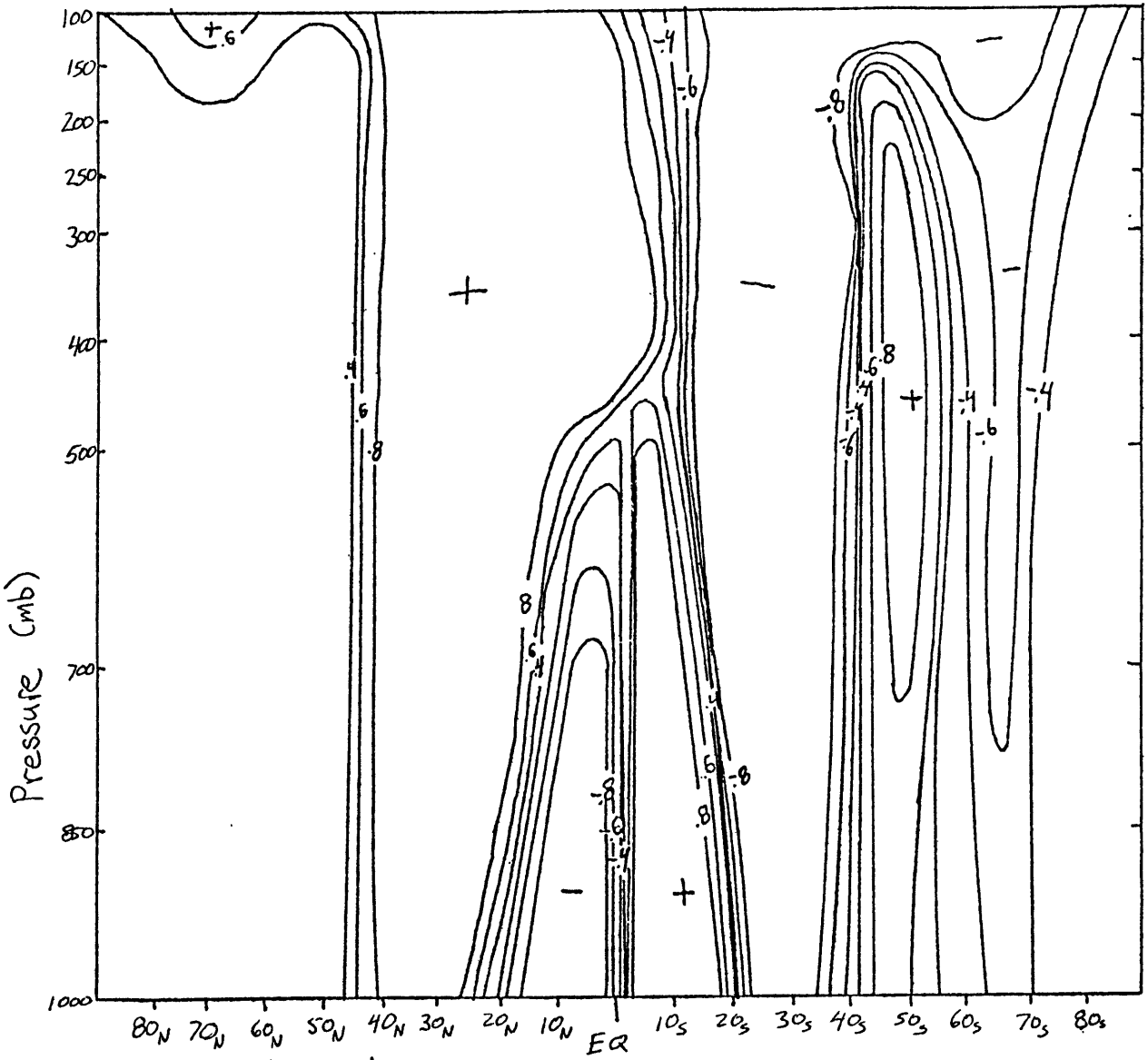

Fig. 3-7. Correlation of [U] vs. EOF 1 time series

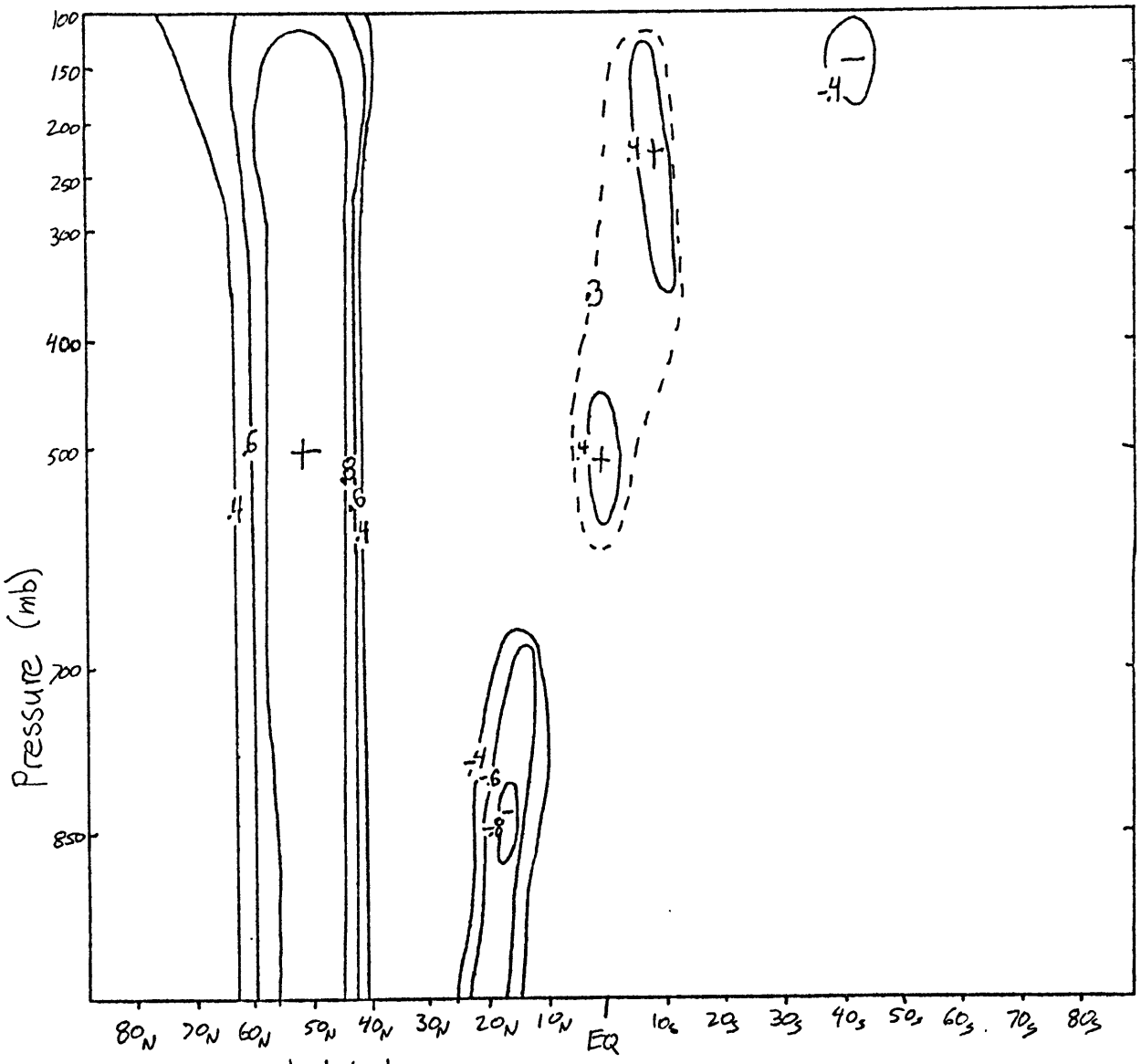

Fig. 3-8. Correlation of [U] vs. EOF 2 time series

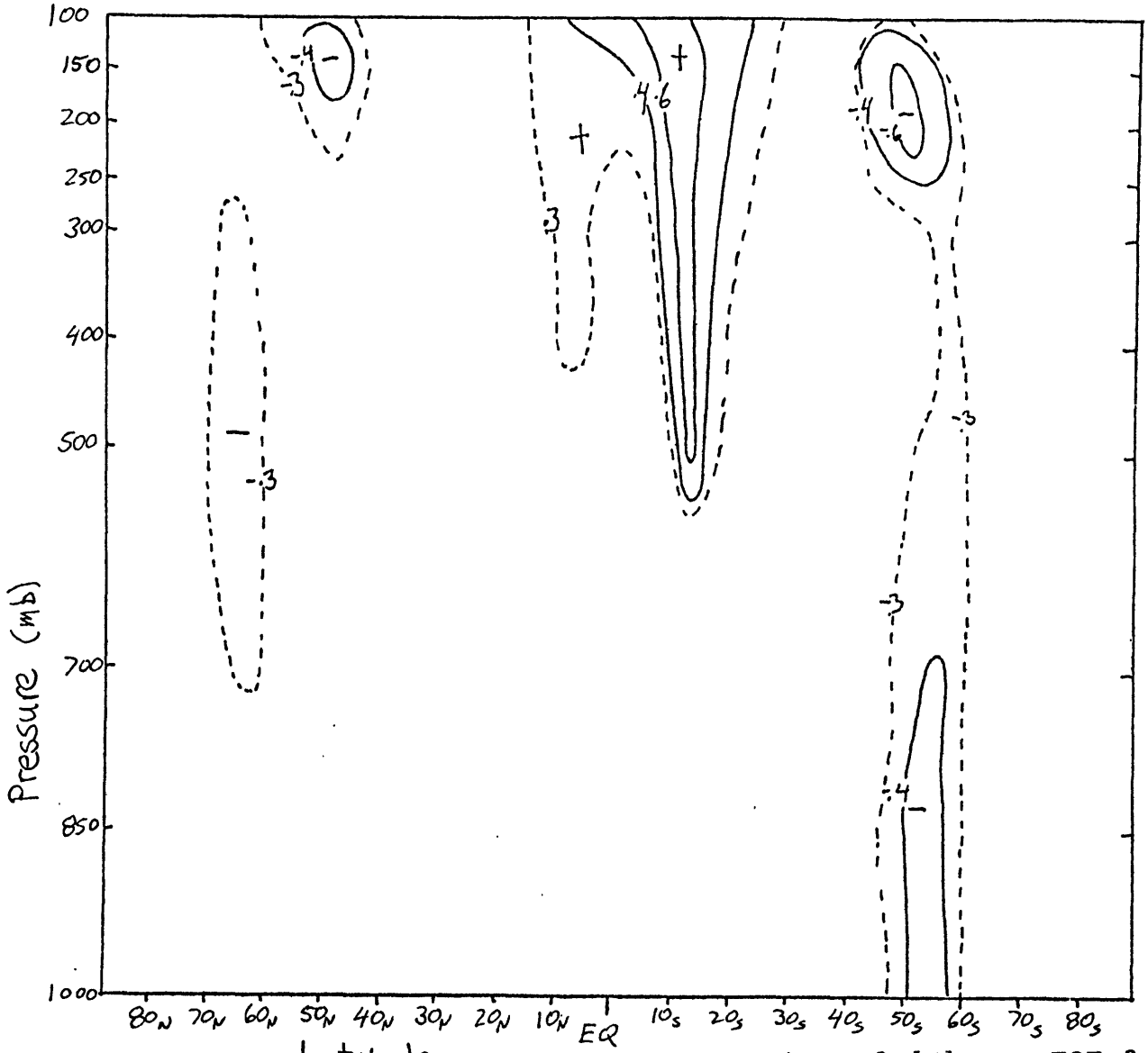

Fig. 3-9. Correlation of [U] vs. EOF 3 time series

divided by the standard deviation of the winds.

Since we are also interested in explaining the M time series, some measure of the contribution of an EOF to the total relative angular momentum is required. The method which I use is to compute M_N, given by [9], which is a normalized measure of the amplitude of M which would result from a motion described by an eigenvector with the amplitude with which it appears in the expansion. This value is a measure of the M series which would occur if the only motion were that which is explained by the particular EOF.

$$M_N = \frac{\sum_{\varphi} \cos^2\varphi \sum_{p} \nabla p(p)\, a_n(\varphi, p)}{\sum_{\varphi} \cos^2\varphi \sum_{p} \nabla p(p)\, a_n^2(\varphi, p)} \qquad [9]$$

The first term of this expression is a measure of the relative angular momentum content of the normalized EOF, and the second term is a measure of its amplitude in the expansion.

The last measure needed is a way of compactly describing the features of an EOF time series. The yearly climatology can be considered to be periodic, so a description based on yearly harmonics as given by [10] would seem to be appropriate.

$$A_n^{\omega} = Amp\left[\frac{1}{2\pi}\sum_t b_n(t)e^{i\omega t}\right]$$
$$Ph_n^{\omega} = Arg\left[\sum_t b_n(t)e^{i\omega t}\right] \qquad [10]$$

Where b_n is normalized as in [8].

Using the measures which are defined above, one can describe the temporal structure of the EOF's. Table 3-1 lists the variance explained, the amplitude and phase of the annual and semi-annual harmonics, the value of M_N for the EOF, and the amplitude of the contribution of the EOF to the annual and semi-annual harmonics of M.

The first EOF clearly explains almost all of the main seasonal cycle from the standpoint of either zonal K.E. or M. A comparison of the first EOF and the annual component of the Fourier decomposition of the zonal wind given by Newell et al. (1974) and reproduced as Figure 3-10 shows them to be very similar as would be expected from the harmonic decomposition of the EOF's time series. An interesting feature of the southern hemisphere annual variation, as shown in Figures 3-3 and 3-7 is the existence of a dipole-like feature caused by the fact that the 45°S-60°S winds are stronger during the southern hemisphere summer than winter. The time series of the second EOF contains terms for the 90° out of phase seasonal component and some of the semi-annual component of zonal K.E., but is not a very important contribution to M. The third EOF, which is very similar to the semi-annual wind decomposition from Figure 3-10, is the major contribution

EOF	% Var	Amp(12 mo.)	Phase(12 mo.)	Amp(6 mo.)	Ph(6 mo.)	$M_n(12)$	$M_n(6)$
1	87.2	4.7	0.16π	0.4	0.79π	3.16	0.26
2	3.6	3.4	-0.34π	2.7	-0.83π	0.55	0.44
3	3.5	1.7	0.64π	4.1	-0.59π	0.38	0.91

Table 3-1
Seasonal Fourier components of EOF time series

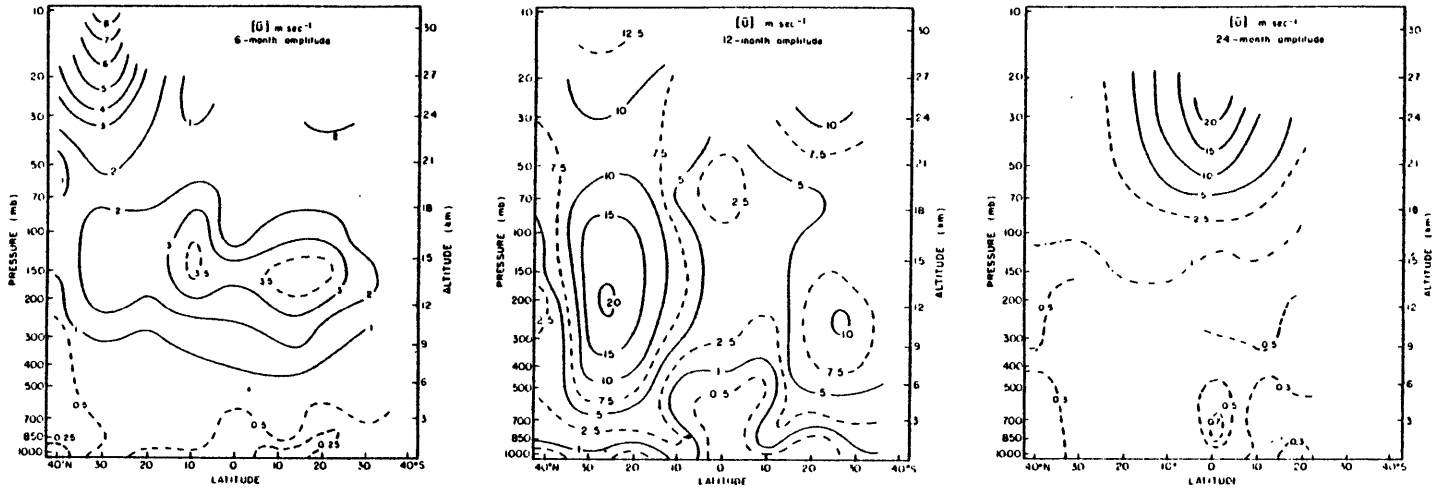

Figure 10.1

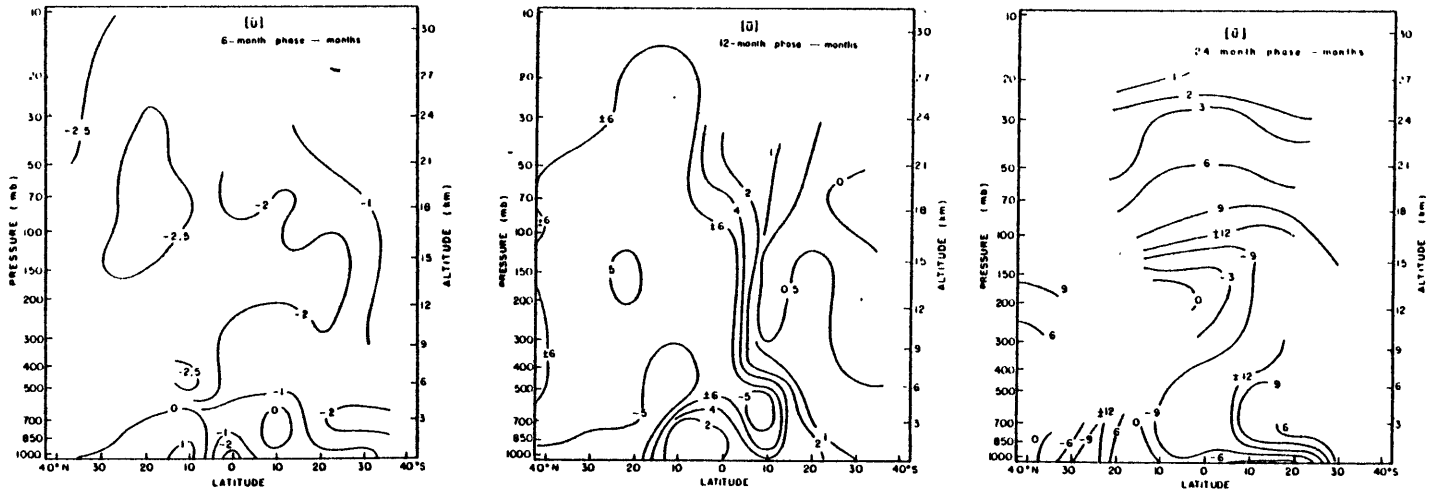

Figure 10.2

Fig 3-10. From Newell et al. (1974)

to the 6 month periodicity in M.

The centering of EOF 3 slightly south of the equator is an interesting, if somewhat puzzling effect. The zonally-averaged data set contains no information on forcing terms so it is not possible to use it to evaluate the physics of this motion. Newell et al. concluded, after examining the momentum budget, that it is probably due to a modulation of the Hadley cell intensity, possibly due to mid-latitude eddy forcing. The southern positioning of the EOF center would also seem to argue for the importance of a southern tropical influence in this motion, perhaps the Southern Pacific Convergence Zone.

THE NON-SEASONAL VARIATIONS

Using the seasonal climatology for the [U] field, it is a simple matter to subtract this from the original time series to produce an anomaly field. A plot of the anomaly time series is given as Figure 4-1. Disregarding the 1976 step, which is discussed in Appendix A, the major variations appear to have time scales greater than 1 year, 'synoptic' scales of less than 10 days, or a 40-50 day quasi-periodicity. As mentioned before the length of the data set is such that it is not possible to adequately examine the low frequency variations. In order to remove the very low frequency content and the high frequency synoptic scale noise, I have constructed a filter with a broad band pass whose frequency response is

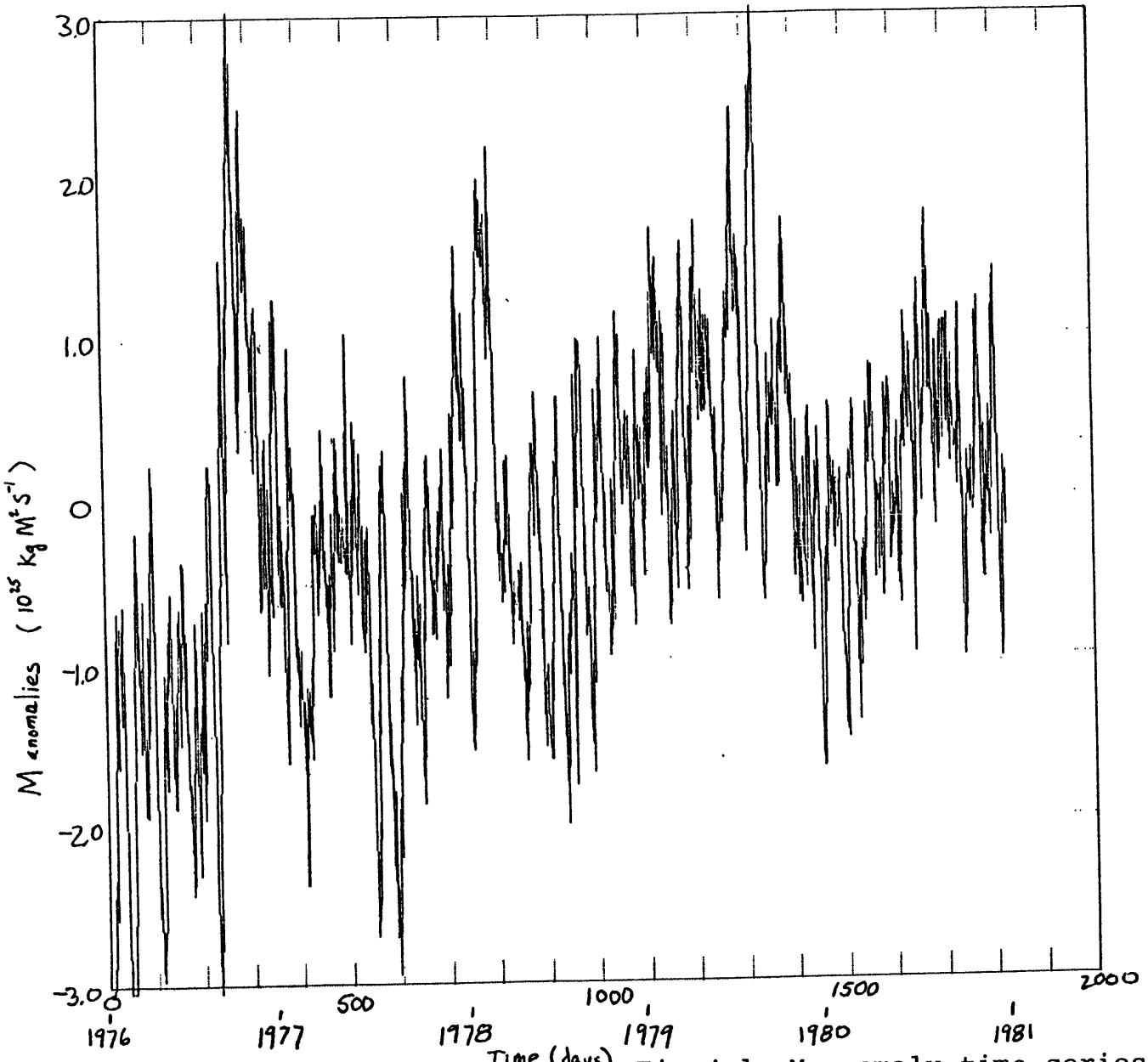

Fig 4-1. M anomaly time series

shown in Figure 4-2. The results of an application of this filter to the M time series is given in Figure 4-3. This plot shows the 40-50 day 'oscillation' to change both frequency and amplitude with no apparent pattern.

In an effort to provide a more concise description of the temporal variations in M, several spectral analysis techniques were used. I will present the results for three of these estimators, a classical Blackman-Tukey (1959) method referred to as B-T, a high resolution autocorrelation based technique due to Capon (1969) and generally referred to as the maximum likelihood method (MLM), and a high resolution autoregressive method due to Burg (1967) and referred to as the maximum entropy method (MEM). Descriptions of the computation of these estimates are given in Appendix B and its references.

The choice of a spectral estimator is a complex question which is dealt with in considerable detail by Kay and Marple (1981). Basically the best choice of estimator is determined by the characteristics of the signal which one is measuring. The classical analysis techniques estimate the spectrum by fitting Z-transform plane zeros, which correspond to spectrum nulls. The autoregressive techniques, and the MLM technique in a somewhat more obscure way, fit Z-transform plane poles, which correspond to spectrum peaks. The classical spectral estimates generally tend to be rather broad with sharp nulls, while the MEM spectra tend to have

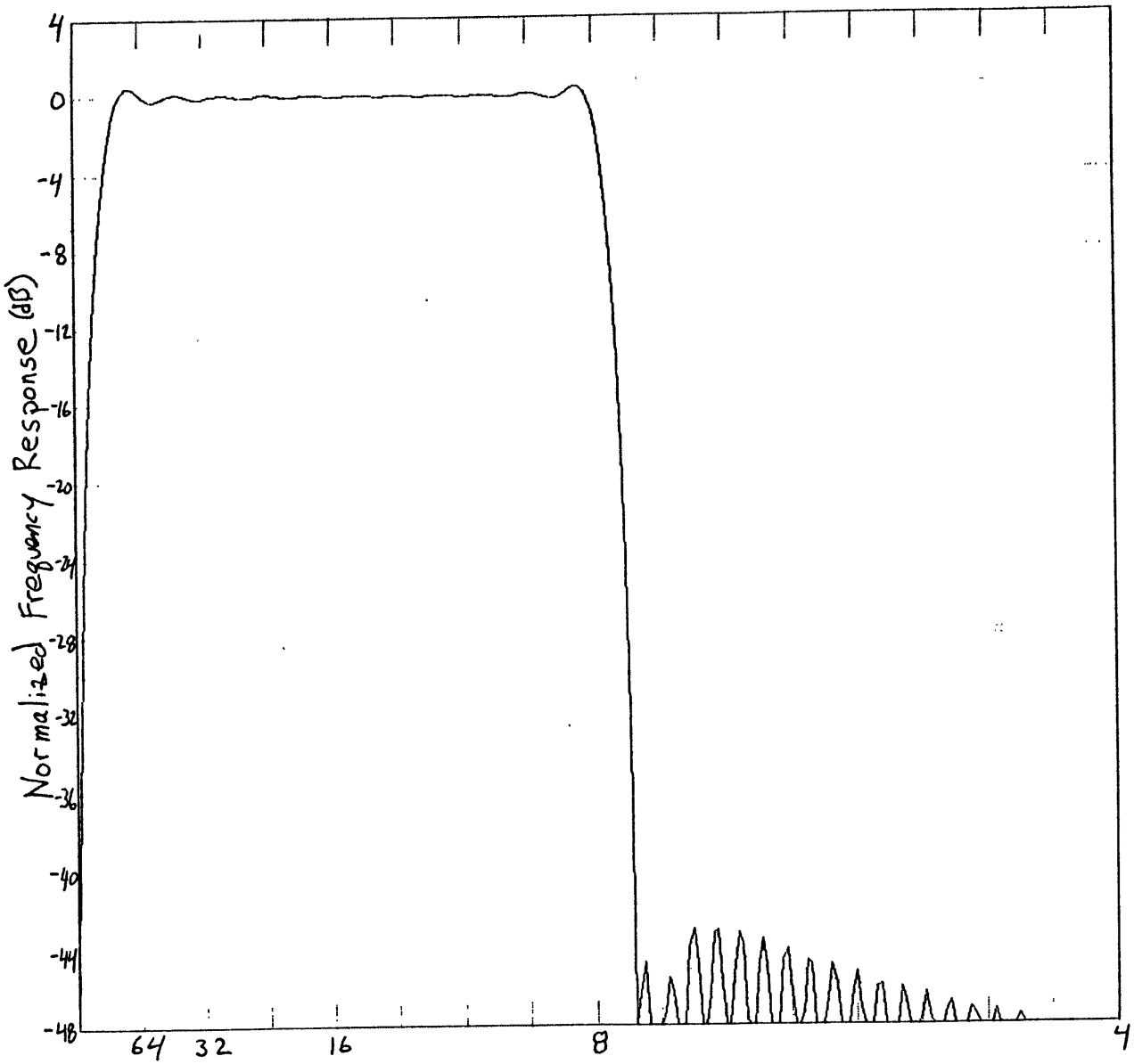

Fig. 4-2. Broad-band-pass filter gain

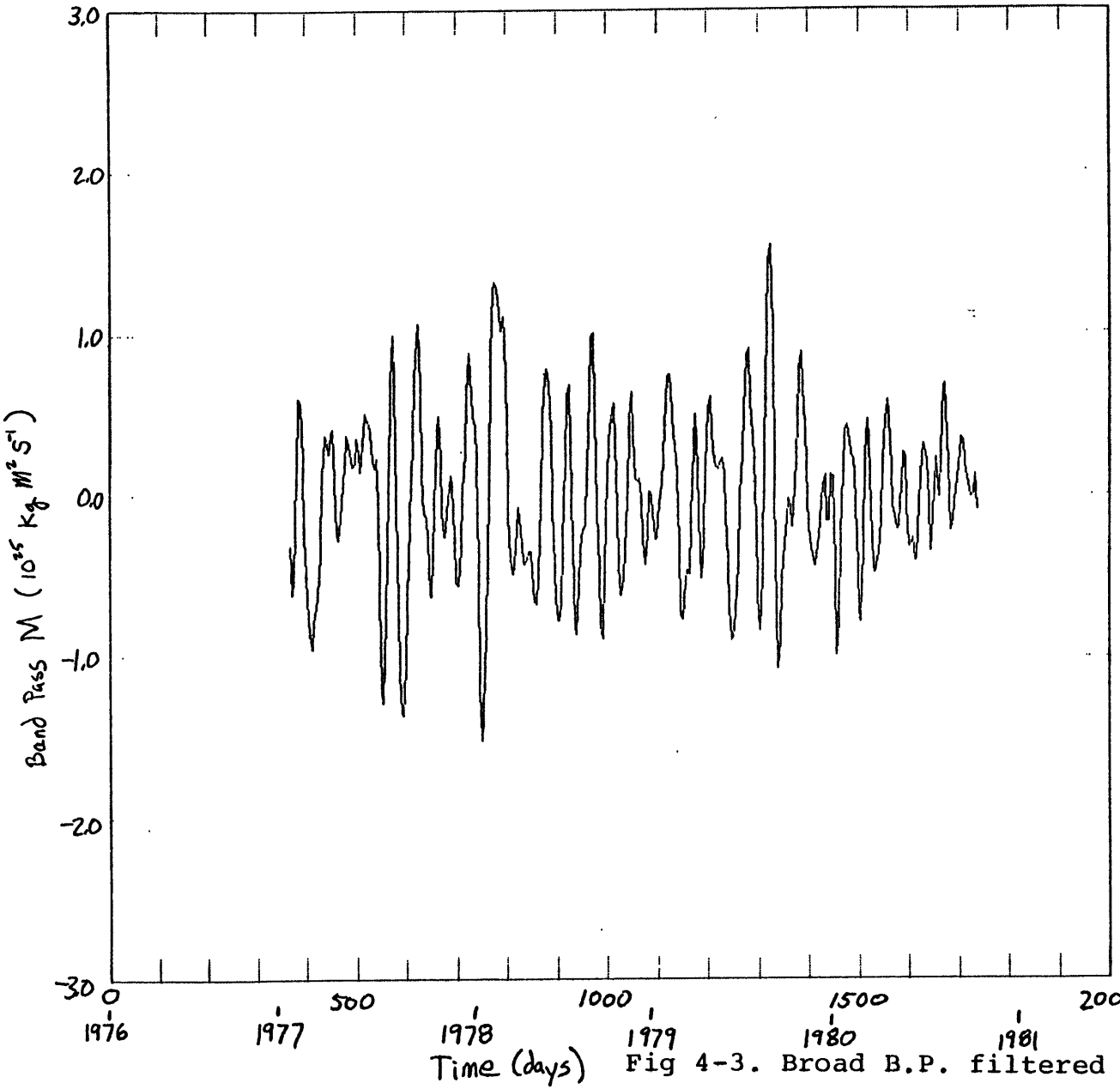

Fig 4-3. Broad B.P. filtered M anomalies

smooth nulls and sharp peaks with good ability to separate narrow band signals, in fact, sometimes creating them even when they are not indicative of the true spectrum. The MLM estimator, which can be considered to be a type of average of N (the autocorrelation order) MEM spectra, is much better than the MEM at representing broad band processes but inferior in separating closely spaced, line-like components.

Estimates of the M anomaly spectra using these three estimators appear as Figures 4-4 to 4-6. The spectra were computed for the part of the sample between day 300 and day 1836 (day 1 = Jan. 1, 1976). The choice of filter order for the MEM estimator is farily critical. The use of too high an order will result in breaking up broad band processes into lines with no real significance. I have attempted to choose an order which adequately describes the singal; however, there are no good objective ways of doing this.

These spectra are consistent with a model possessing a poorly resolved low frequency component, and a relatively broadband peak at frequencies corresponding to 40-50 day periods. The spectra also seem to show some evidence for power at 17- and 12-day periods. These higher frequency components have significant coherency values in some of the computed cross spectra but efforts to describe a coherent spatial structure have been hindered by the very small amount of power in these lines.

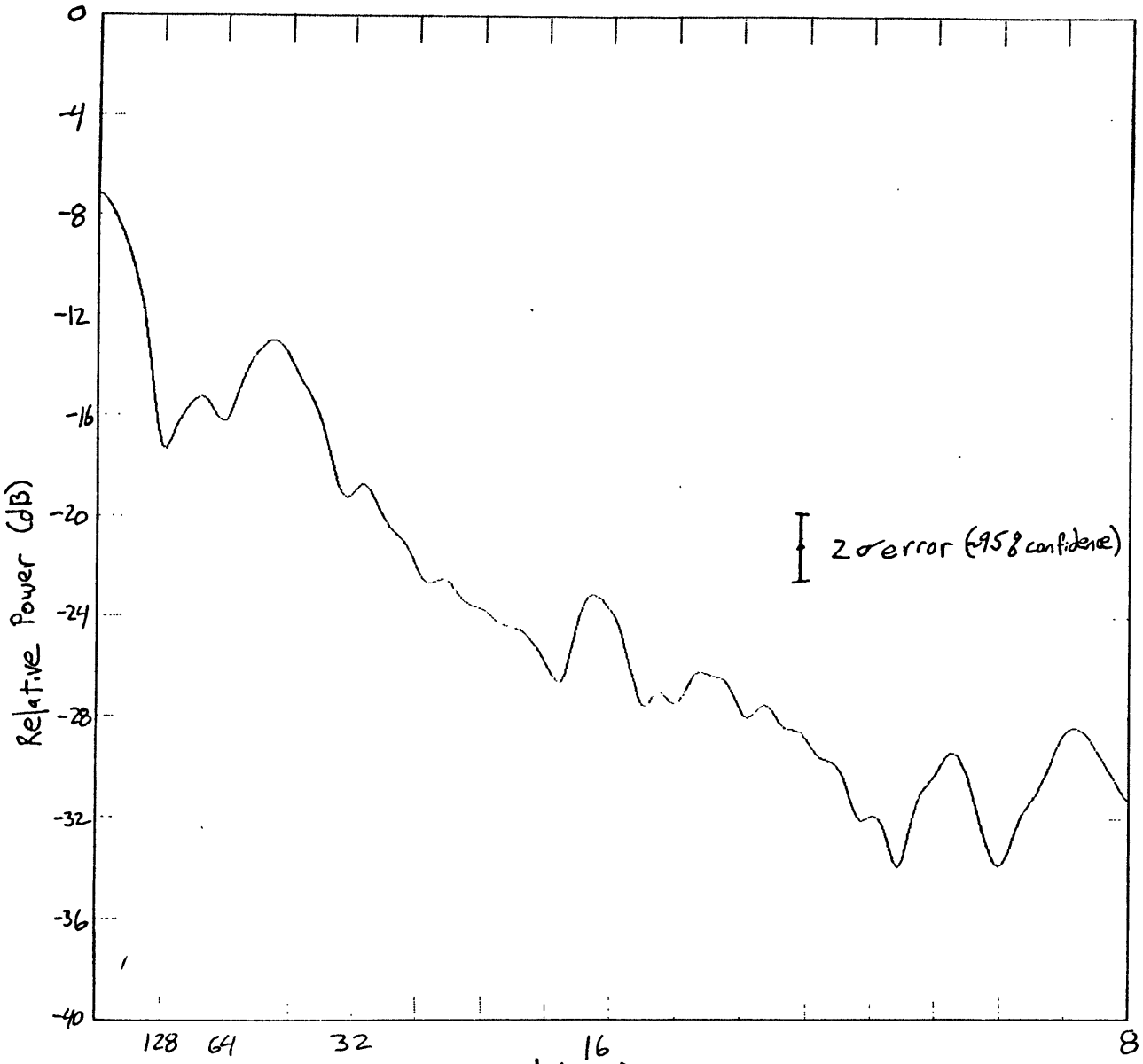

Fig. 4-4 B-T power spectrum of M anomalies

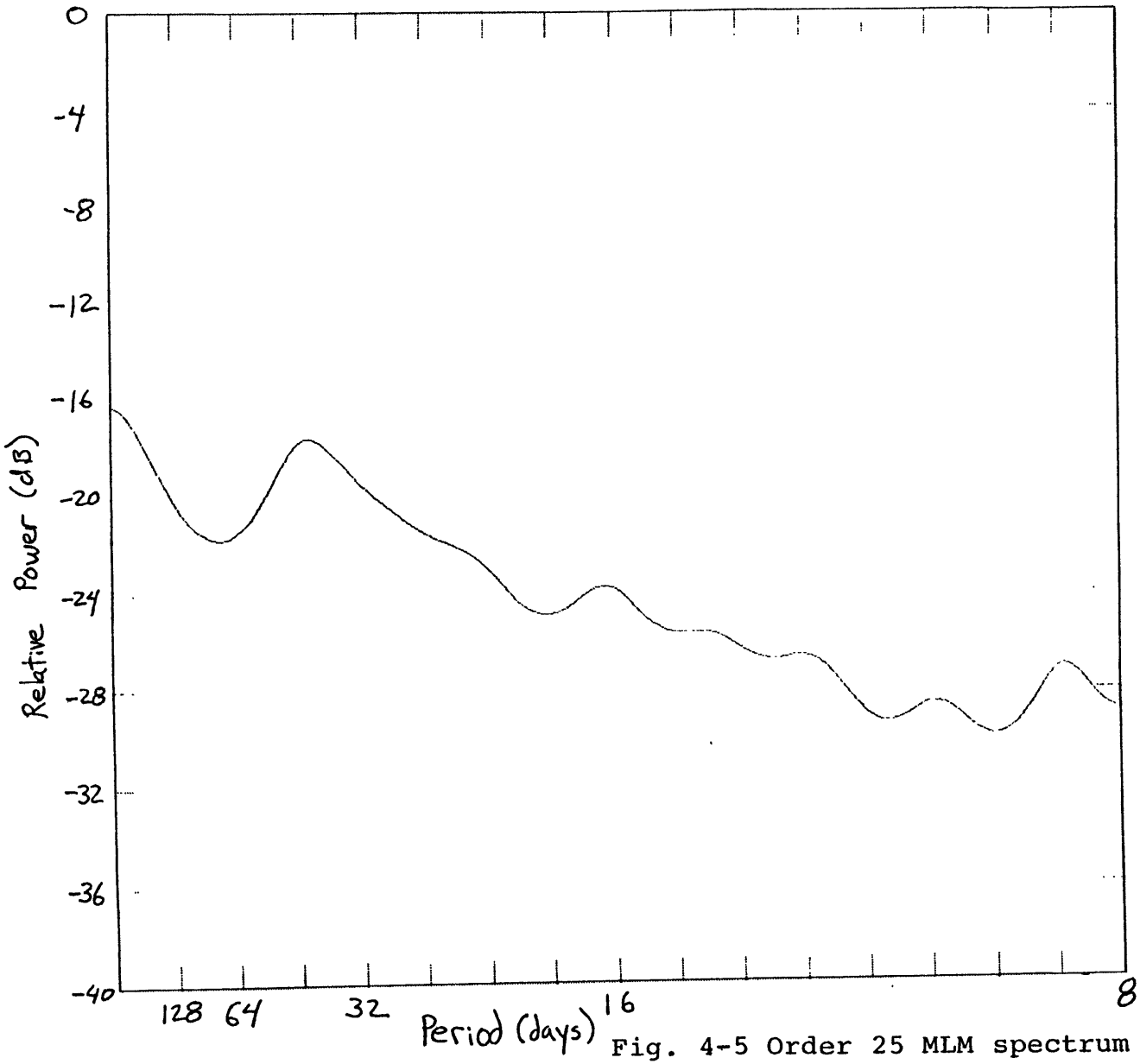

Fig. 4-5 Order 25 MLM spectrum

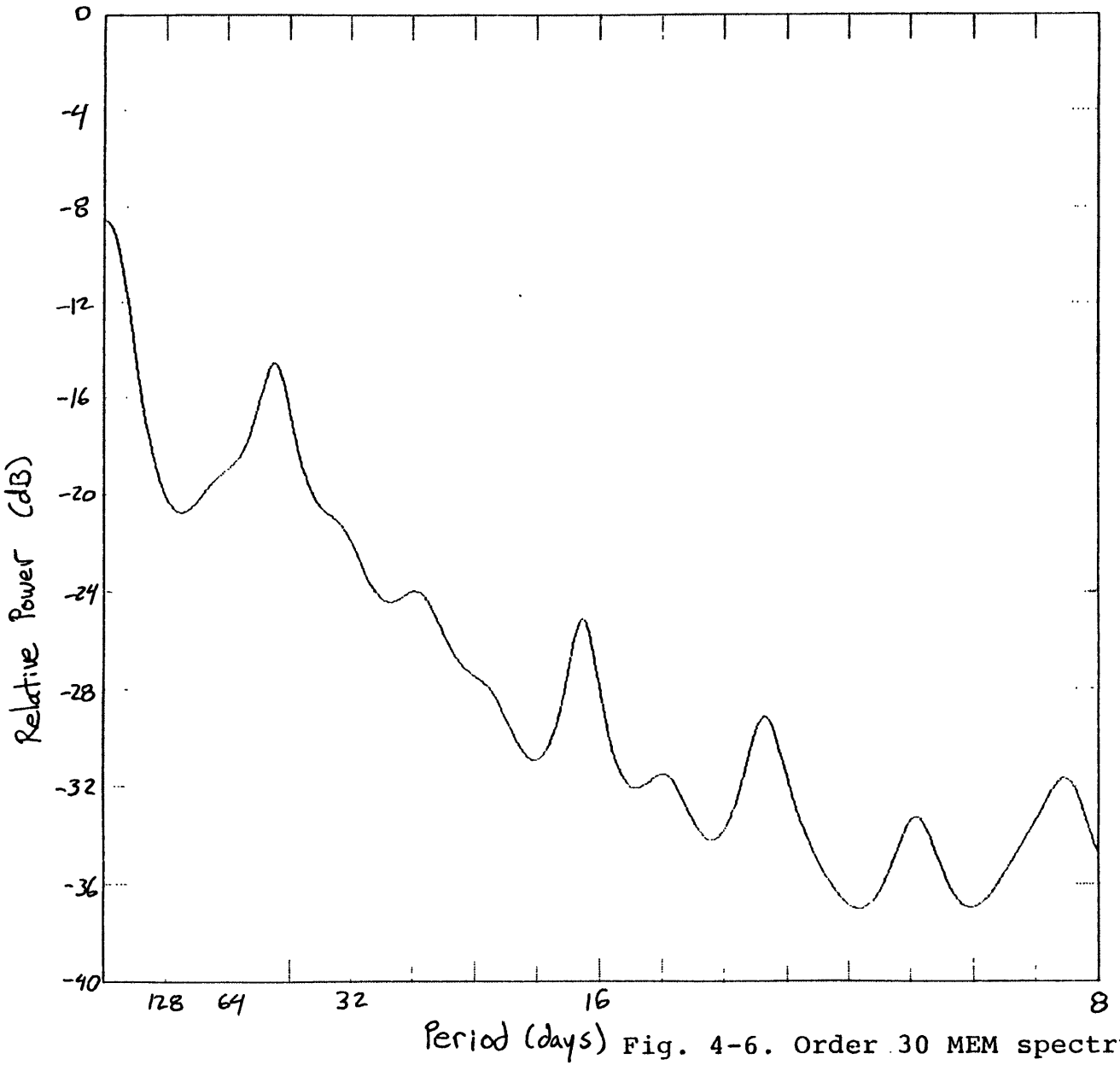

Fig. 4-6. Order 30 MEM spectrum

A logical next step in studying the 40-50 day variations is the construction of a time series which isolates the motion. This was done with a Hamming window based linear filter whose frequency response is shown as Figure 4-7. The impulse response length of the filter is 179 points and the effective correlation length of the output series is about 100 days giving a Nyquist sampling rate of 50 days. The filter is normalized so that its peak gain is 1.0.

Plots of the filtered time series and the standard deviation of the filtered [U] field are given in Figures 4-8 and 4-9. The spatial distribution of the 40-50 day band pass standard deviation looks very similar to that of the anomalies themselves, indicating a need for somewhat more elaborate processing to reveal a spatially coherent structure, if it exists. I will show the results of some of these techniques in the next section.

THE SPATIAL STRUCTURE OF THE 40-50 DAY 'OSCILLATION'

The presence of 40-50 day tropical wind and surface pressure variations was first observed by Madden and Julian (1971) and later described in somewhat more detail in Madden and Julian (1972). Surprisingly, as far as I can tell, no more recent observational studies of this phenomenon have been published. There has been a considerable amount of theoretical work, mostly attempts to explain the motions as linear equatorial Kelvin waves (Chang 1977 and others). Madden and

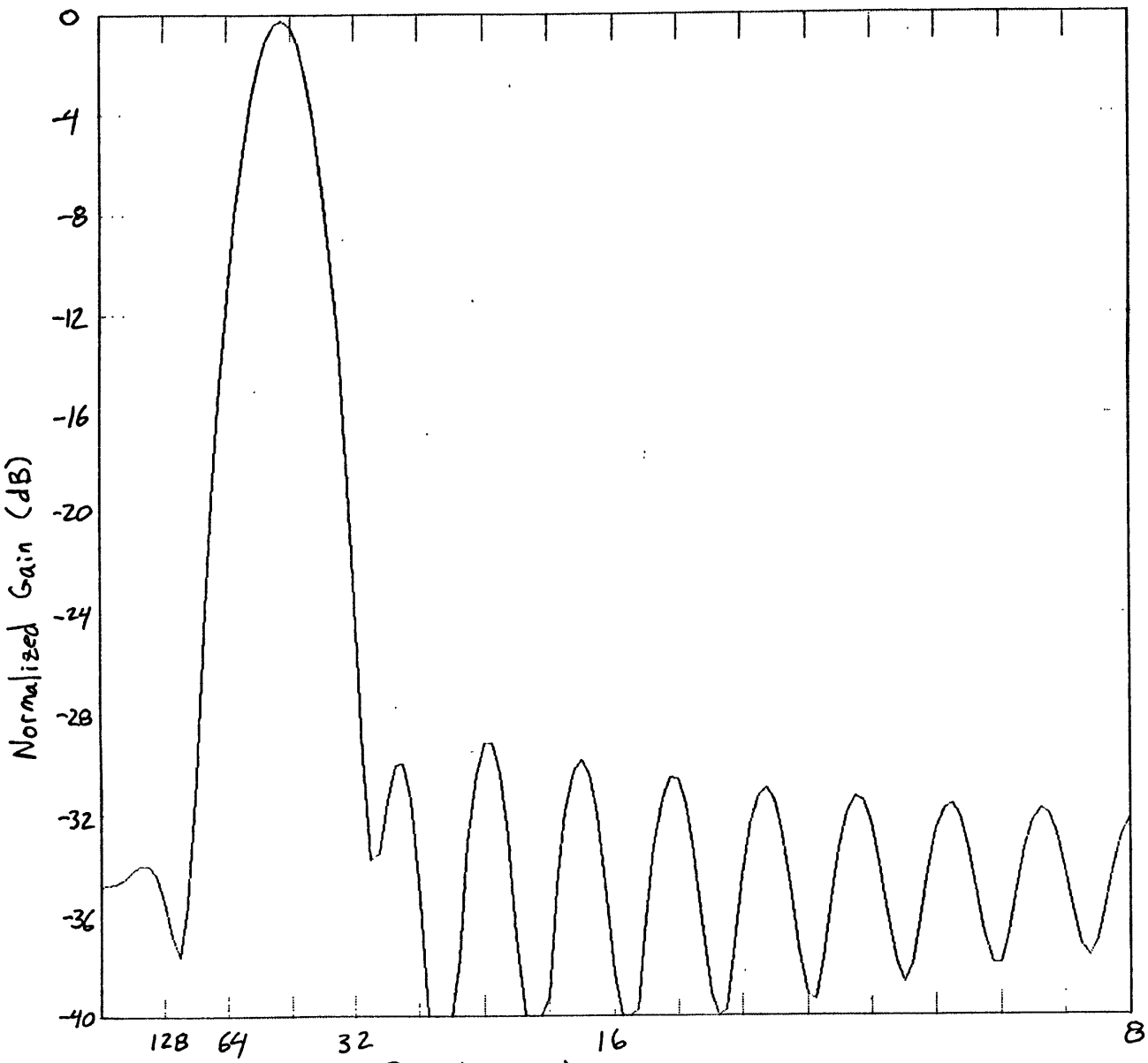

Figure 4-7. 45 day band-pass filter gain

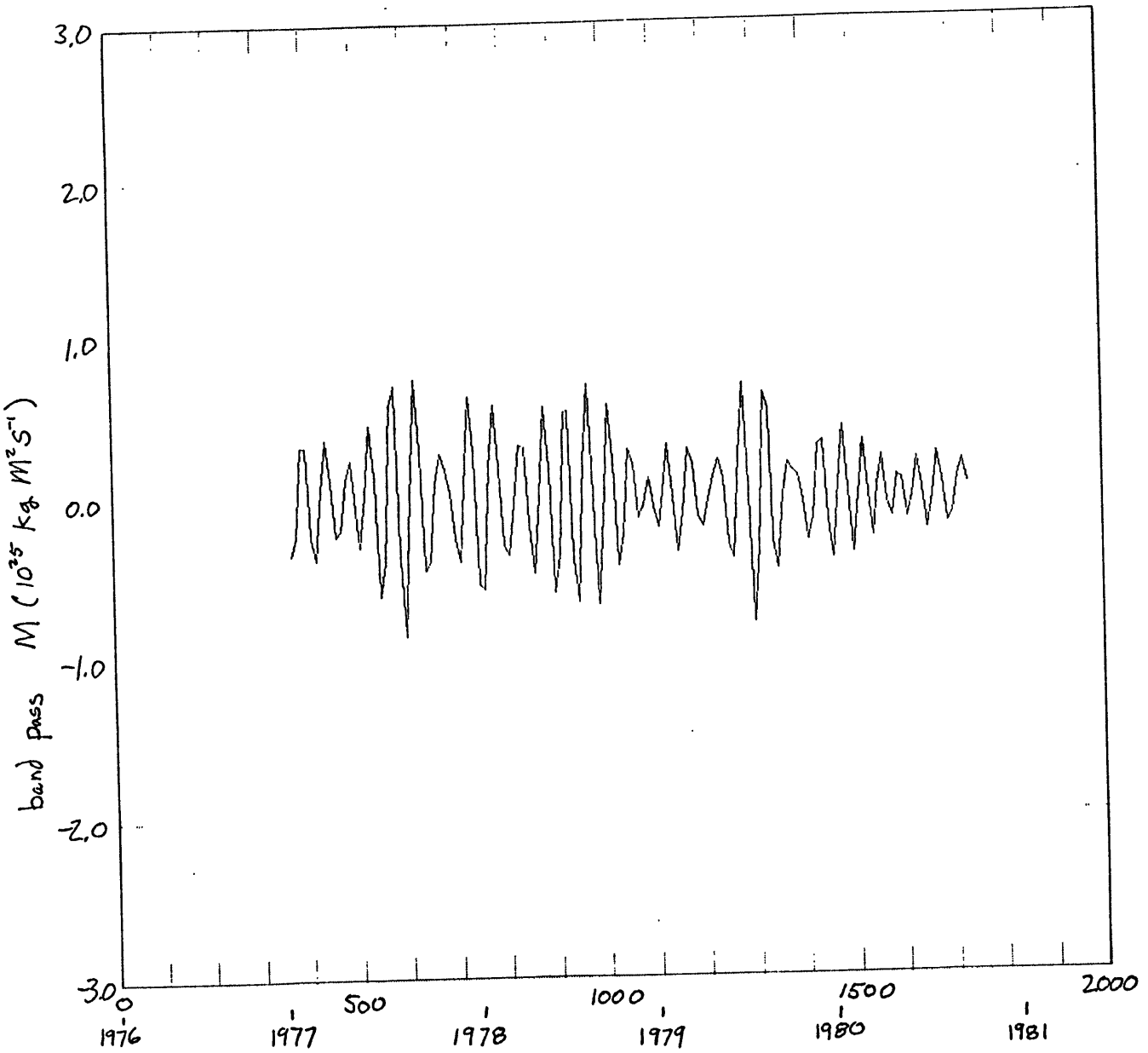

Fig. 4-8. 45 day B.P. M anomalies

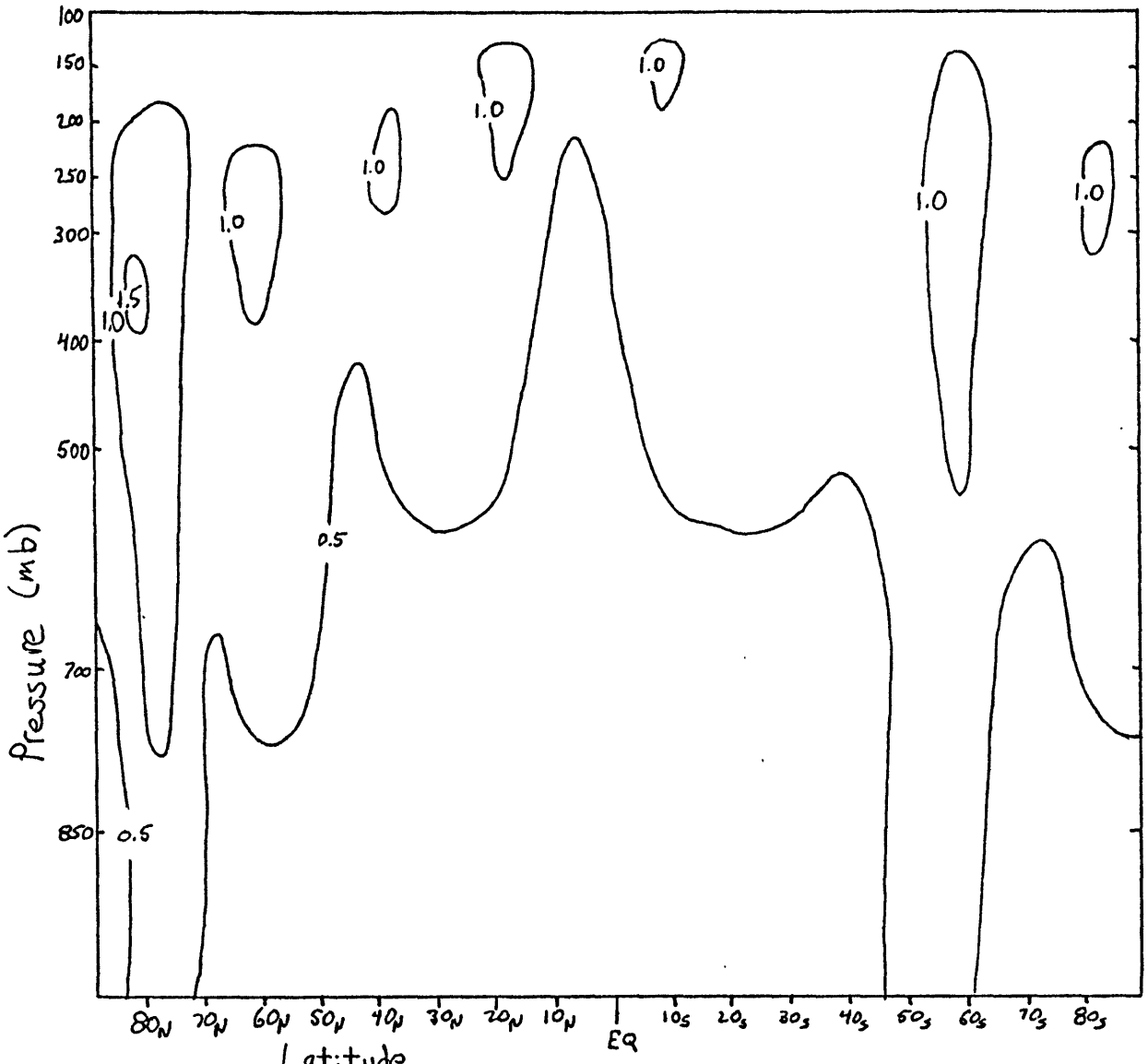

Fig. 4-9. Std. Dev. 45 day B.P. [U] anomalies

Julian (1972) describe the surface pressure variations as a wave-like disturbance with eastward and poleward phase propagation. They found the amplitude of the oscillation to increase as the disturbance travelled over the tropical west pacific. It is this modulation which probably causes the associated time variations in M and [U] as a pure travelling wave would make no contribution to the zonally averaged quantities. Madden and Julian searched for but were unable to find an influence of this oscillation in the northern pacific surface pressure records. They also examined zonal winds from a small number of the IGY radiosonde stations, some of which showed limited evidence of vertical phase propagation, while some showed an abrupt sign reversal at a mid-tropospheric height.

In order to describe motions with propagating phase it is necessary to extend the analyses used in the section on seasonal variations. To do this an orthogonal version of the filitered data set was constructed by phase shifting each component of the series 90°. Such a series is generally referred to as a Hilbert transform of the filtered series (Oppenheim and Schafer 1975). There are some non-obvious issues involving the orthogonality of such a transform in a sampled realization, which are discussed in Appendix C. Appendix C also discusses the extension, using the Hilbert transform series, of the correlation and EOF analyses for the production of amplitude-phase fields.

Figures 5-1 and 5-2 show the correlation amplitude and phase for the band pass filtered [U]'s vs. the M series computed from the same data. In classical terms the correlation coefficients are equivalent to the coherency of the cross spectrum of the time series vs. the resolution cell time series at the 45-day period. In those terms the cross-spectra have about 60 degrees of freedom yielding a 95% confidence interval for correlations slightly greater than 0.4 (Goodman et al., 1961). The sign convention is such that the phase propagation is in the direction of increasing phase.

The pattern indicated by this analysis is one of a coherent tropical motion where the high altitude equatorial winds lead the M series and the phase propagation from there is poleward and downward. The structure of the correlation amplitudes shows two tropical maxima spanning the equator, with the center slightly north of the equator, but otherwise very similar to the structure of the semi-annual variation. The northern hemisphere results show a well-defined phase propagation to 45 north and a dipole like structure north of that. The southern part of this dipole is approximately 180° out of phase with the equator and the northern part is essentially in phase. The northern hemisphere correlations show almost no vertical phase propagation. The southern hemisphere correlations are quite different from the northern hemisphere with a sharp drop in correlation and a halt in the southward phase propagation at about 20°S. An important question which

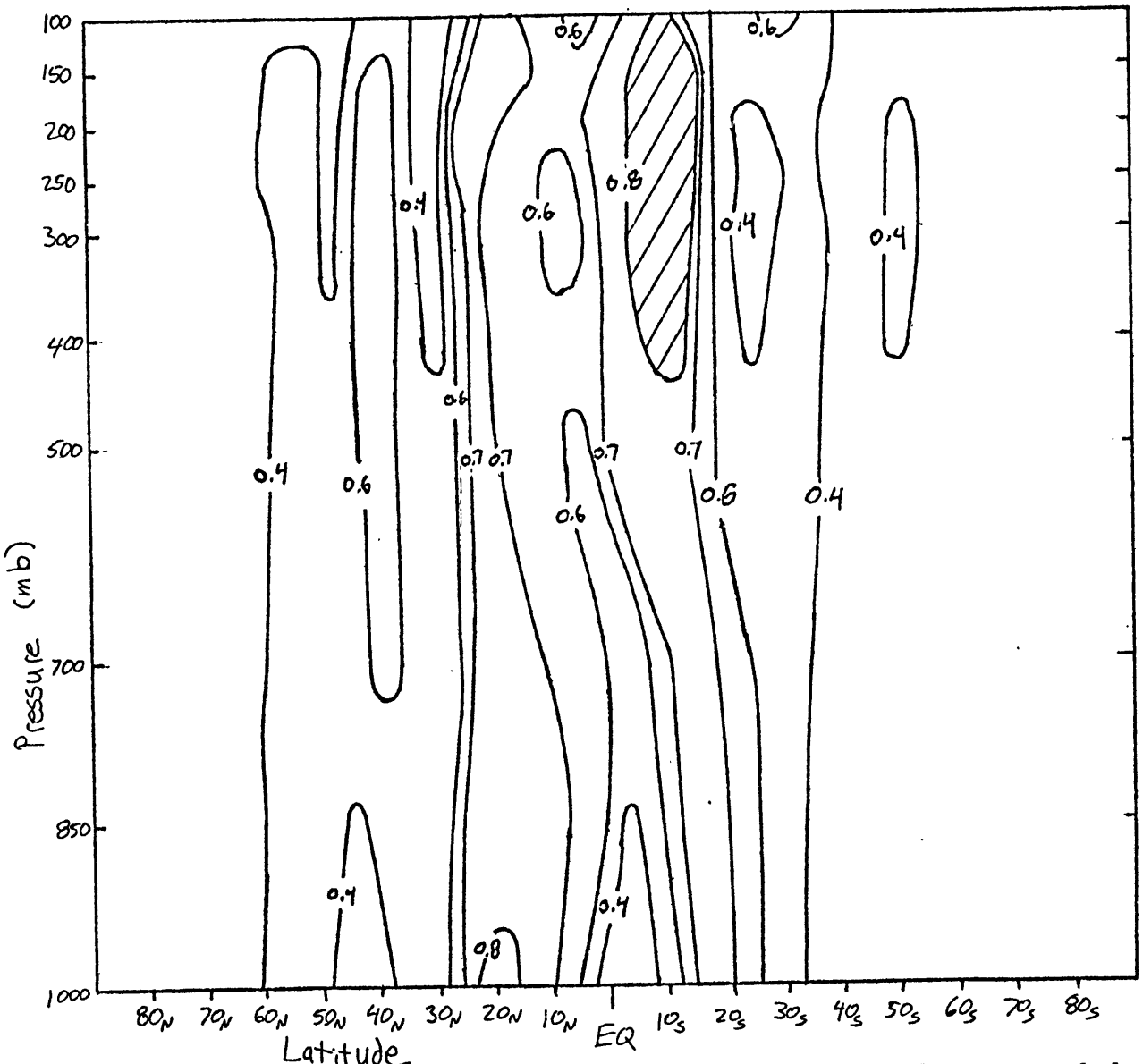

Fig 5-1. Corr. Amp. for 45 day B.P. [U] vs. M

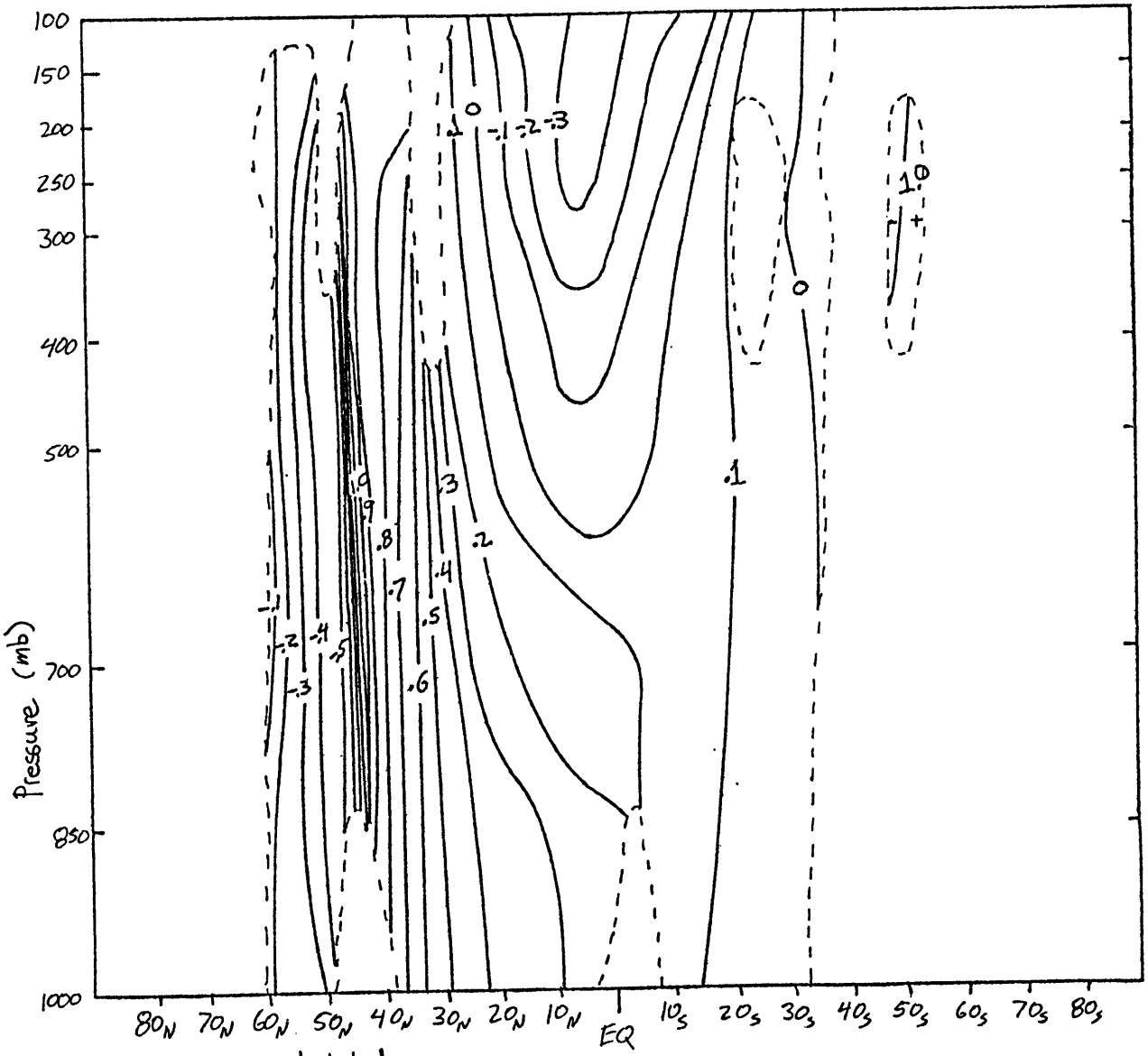

Fig. 5-2. Corr. Phase for 45 day B.P. [U] vs. M

I have not answered is whether this lack of southern hemisphere correlation is the result of different physics or is simply due to a much poorer analysis than the northern hemisphere. The first amplitude-phase EOF of the band pass filtered winds explains 36% of the variance and is shown as Figures 5-3 and 5-4. Figure 5-5 shows the correlation of the [U] field with the EOF time series. The absolute phase of the EOF is arbitrary. The pattern revealed is very similar to that of the correlation with the M series, with somewhat higher correlation values, particularly in the northern hemisphere. This is not surprising as the EOF time series is in some sense optimum. To determine the significance of the tropical-northern hemisphere connection, several point to point cross-spectra were computed. The results for two of these are included in Table 5-1.

The second amplitude-phase EOF (Figures 5-6 to 5-8) explains 22% of the variance and shows a very coherent southern hemisphere structure with poleward phase propagation from 20°S to 40°S and constant phase from 50°S to 70°S. This is a very interesting structure, but I feel that further investigations should use a more appropriate data set for the study of a southern hemisphere high latitude feature.

DICSUSSION AND CONCLUSIONS

The major results of this work are the creation of a new observational description of the tropical 40-50 day

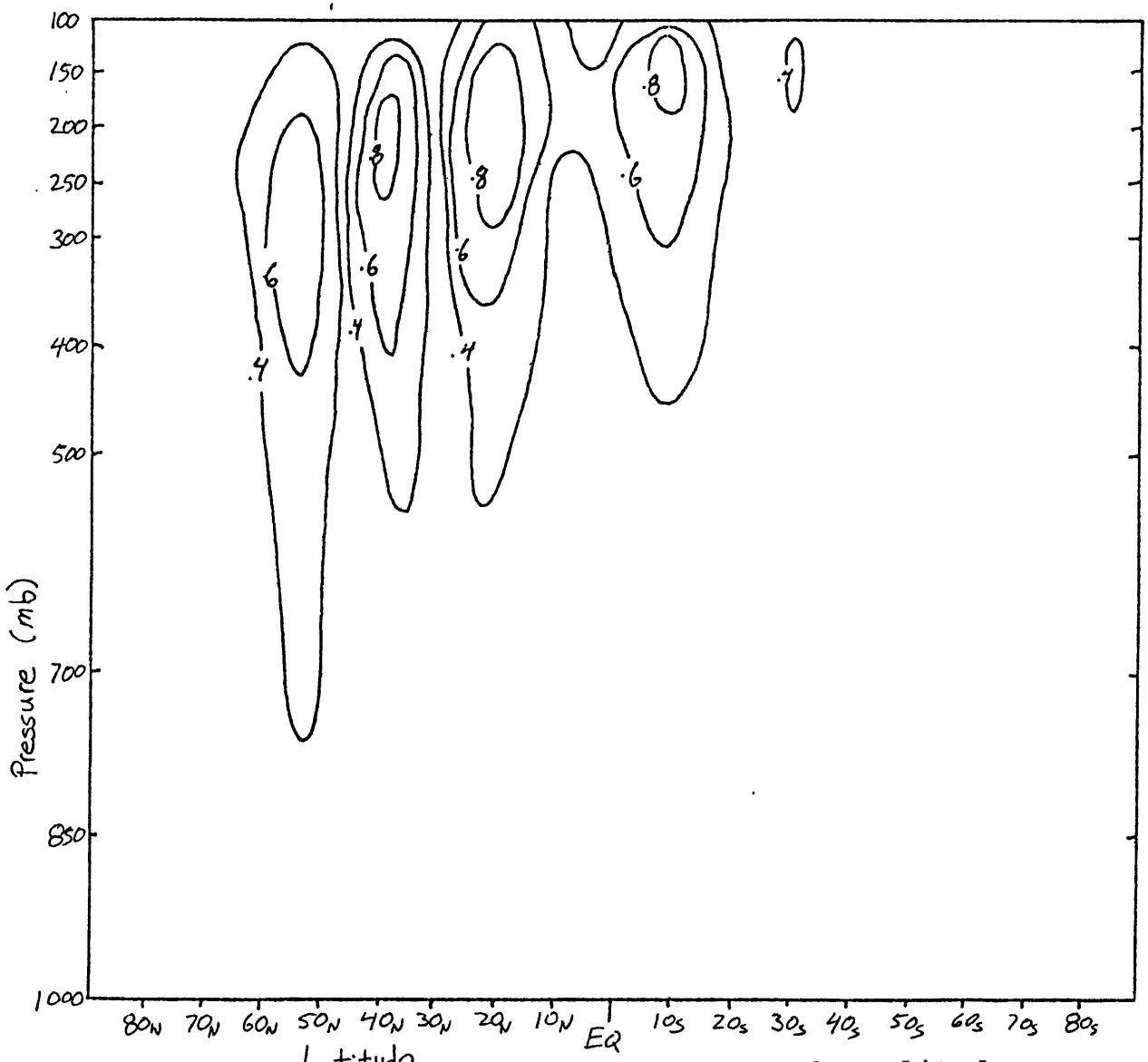

Fig. 5-3 45 day EOF 1 amplitude

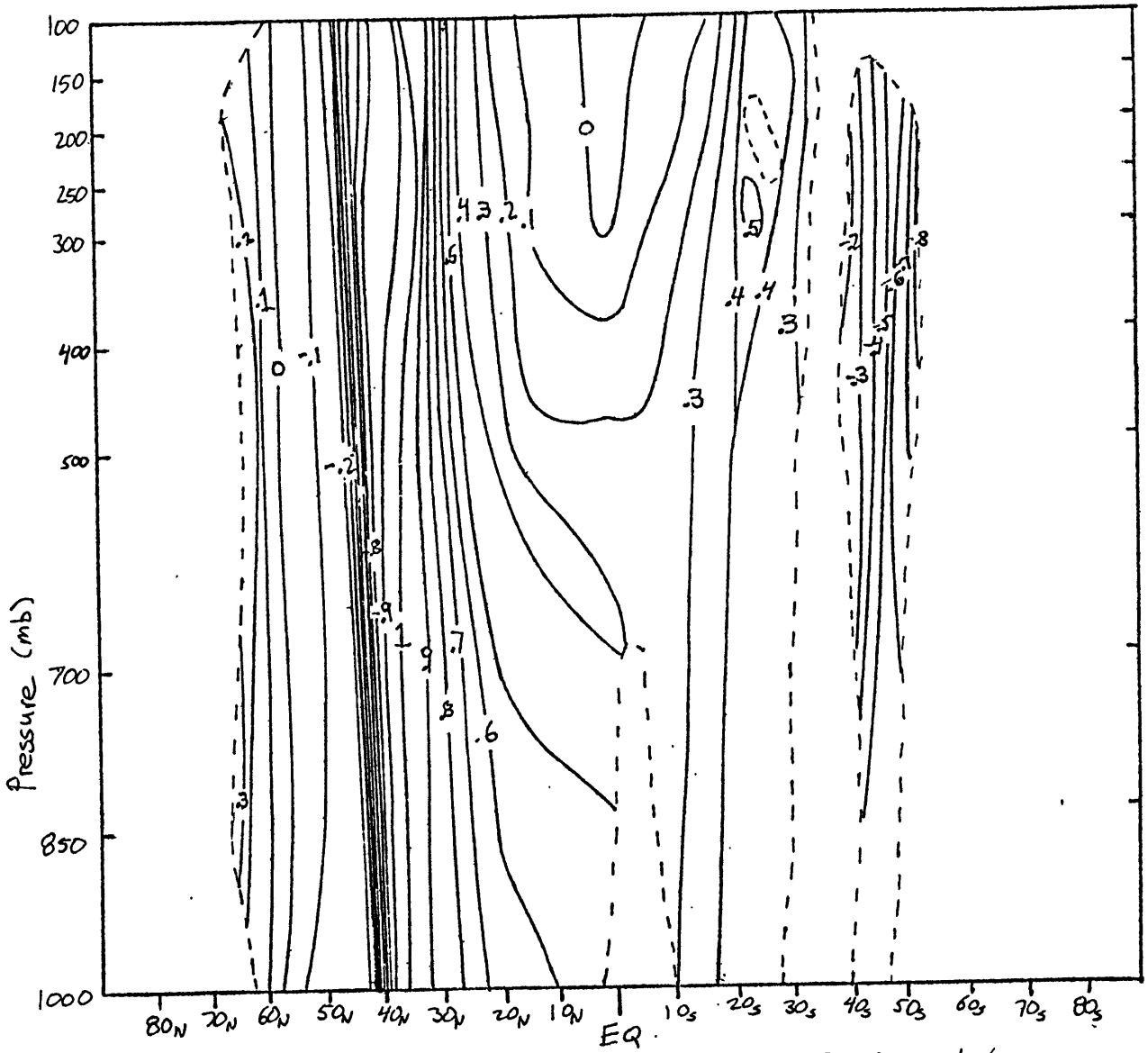

Fig. 5-4 45 day EOF 1 phase/π

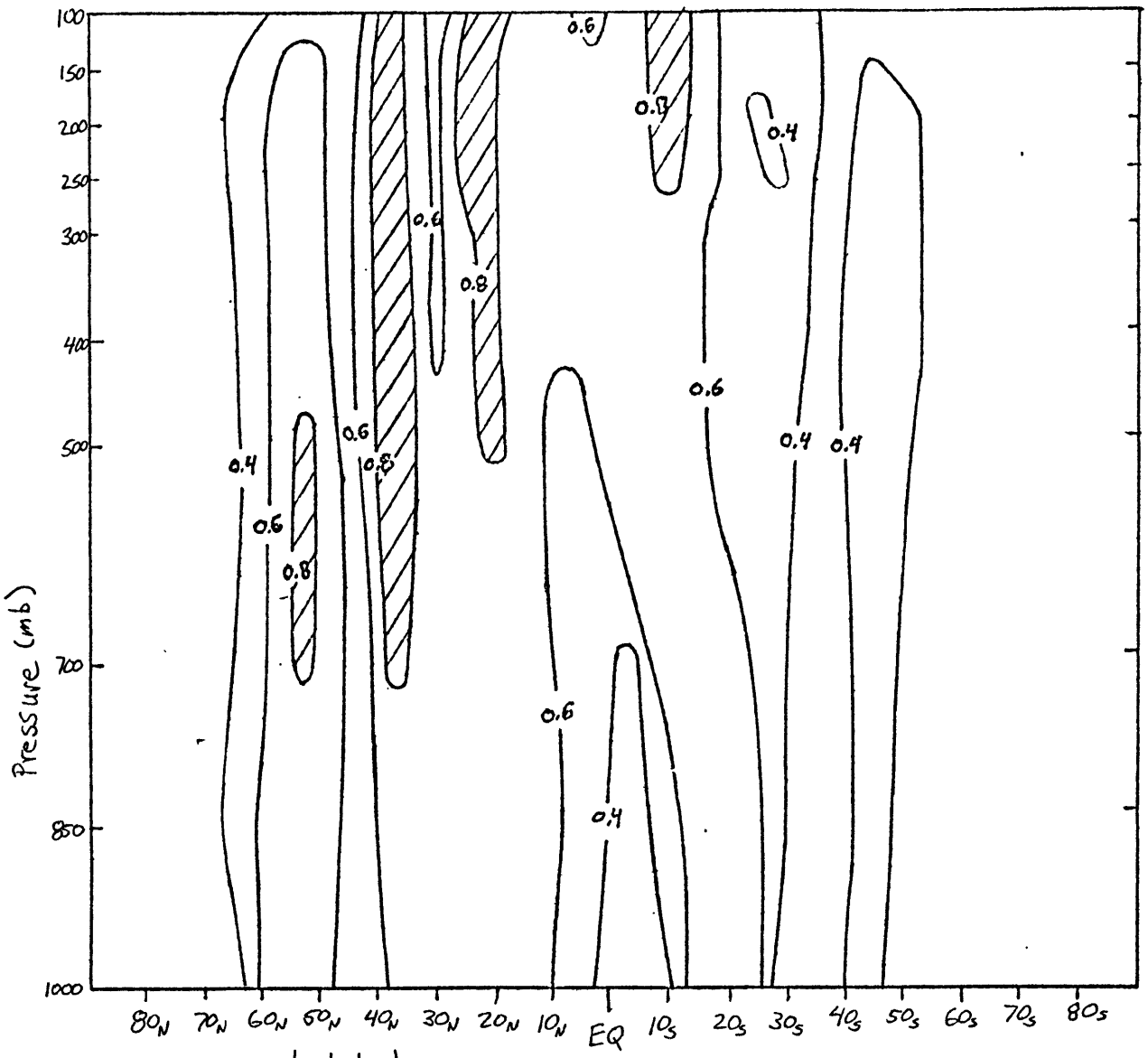

Fig. 5-5. Corr. Amp. EOF 1 time series vs. [U]

	20°N, 250 mb. vs. 37.5°N 250 mb.		37.5°N, 250 mb. vs 50°N 700 mb.	
Period (days)	Coh^2	Phase/π	Coh^2	Phase/π
160	0.46	0.89	0.34	0.95
80	0.43	0.93	0.40	-0.95
53	0.52	0.93	0.42	0.95
40	0.69	0.91	0.53	0.80
32	0.47	0.96	0.26	0.92
26	0.12	-0.91	0.25	-0.92
22	0.05	-0.91	0.25	-0.99
20	0.03	0.96	0.22	0.86
18	0.10	0.98	0.23	0.73
16	0.04	0.77	0.25	0.80
15	0.12	0.62	0.27	0.86
13	0.03	0.60	0.32	0.95

Table 5-1

Cross spectra of [U] anomalies. For 95% confidence $Coh^2 \sim 0.29$

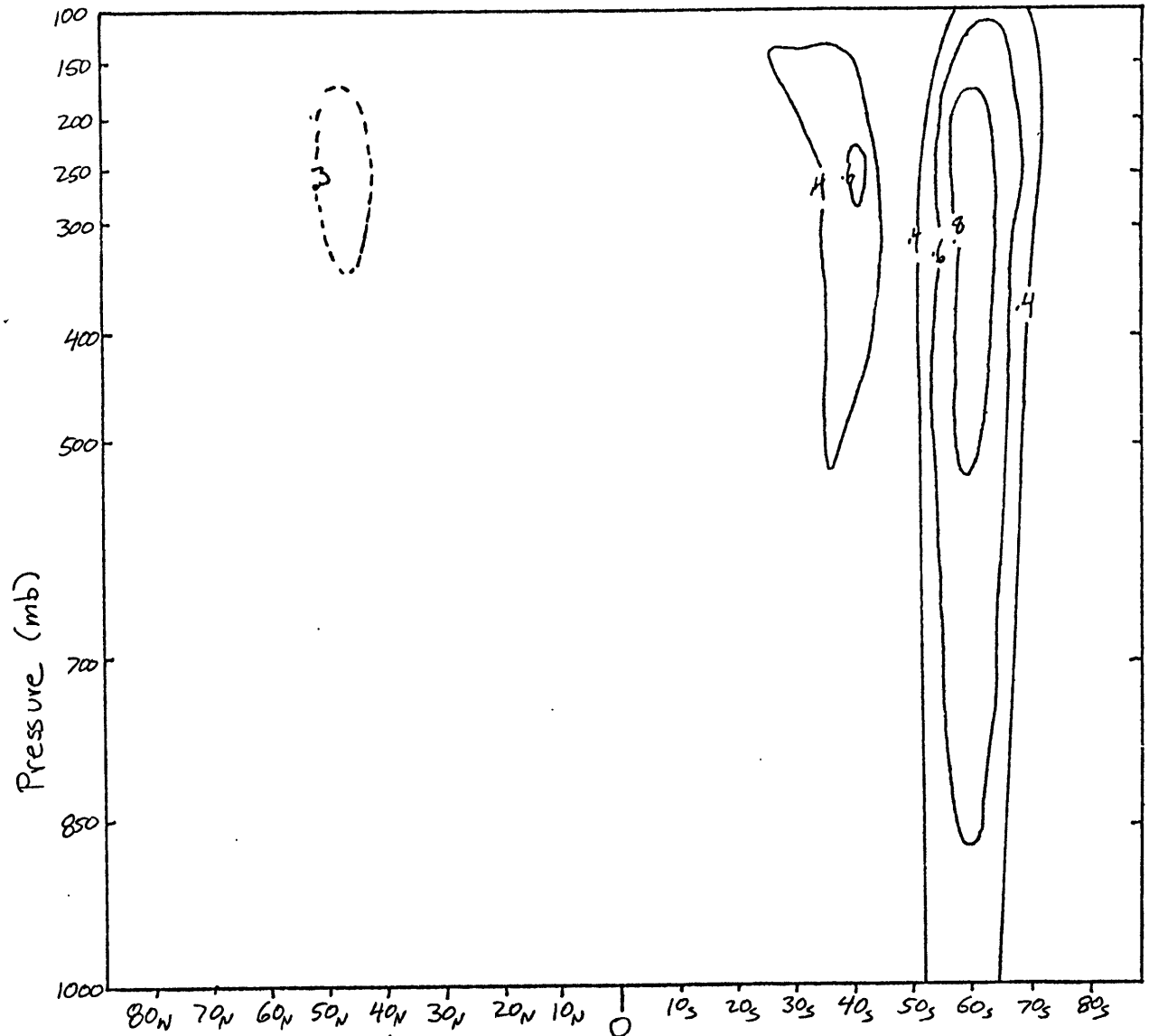

Fig. 5-6 45 day EOF 2 Amplitude

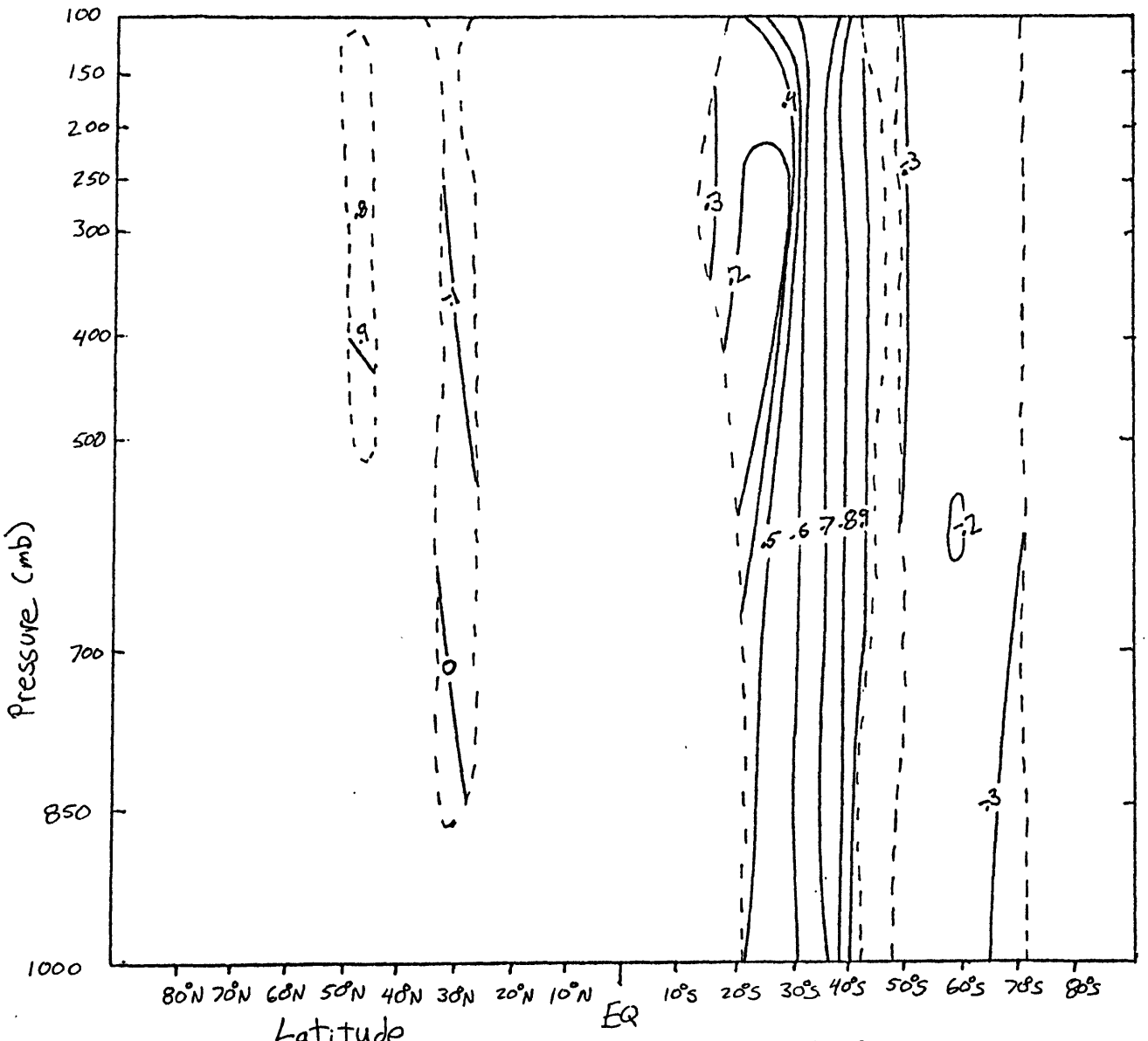

Fig. 5-7. 45 day EOF 2 phase/π

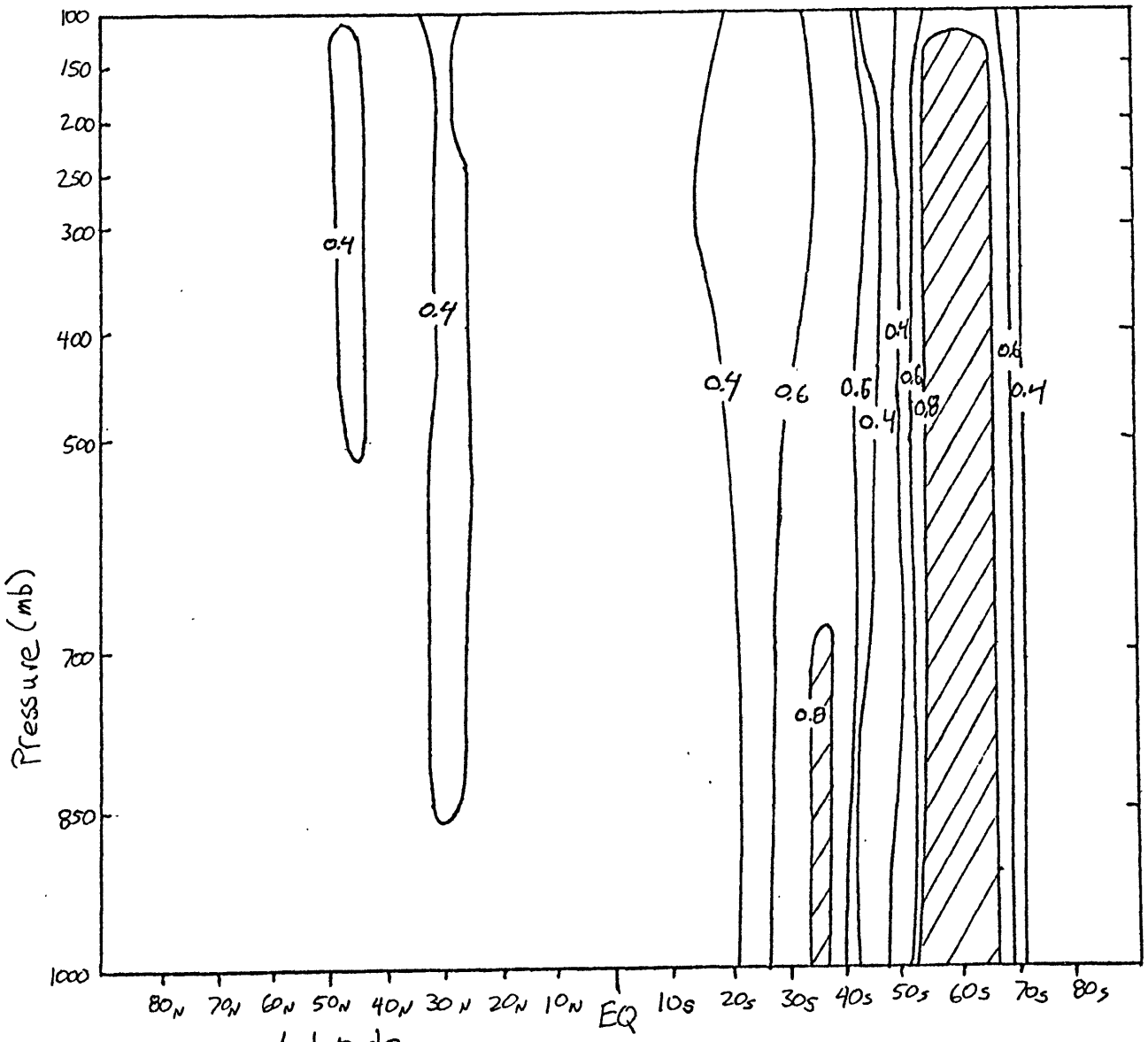

Fig. 5-8. Corr. Amp EOF 2 time series vs. [U]

variations discovered by Madden and Julian and the discovery of associated northern hemisphere changes. Madden and Julian suspected that there might be a mid-latitude component but failed to find one in the north pacific surface pressures. This was probably because the nature of the northern hemisphere response appears to be a shift in the positions of zonally-averaged temperature gradients, resulting in a change in the thermal wind pattern. It is not necessary for such a change to be accompanied by a large change in surface pressure. To make such a change in the zonally-averaged temperature field would seem to require a variation in the energy fluxes due to the general circulation.

All the important motions for fluxes in the mid-latitudes involve eddy terms which do not appear in the zonally-averaged field and can not be seen in this data set. To describe the mechanism by which these connections are accomplished will probably require a study of the 3-dimensional wind and temperature field. However the well-defined phase propagation and the existence of the equatorial component as a coherent phase reference should make the search considerably easier.

The amplitude-phase EOF description of the tropical component of the oscillation is somewhat more detailed than that of Madden and Julian in that it describes a definite downward phase propagation of the motion. This should be useful in assessing the results of analytical work,

particularly the linearized Kelvin wave model of Chang (1977), which was commented on by Stevens and White (1979), where the vertical phase structure of the observed motion is important. The similarity of the tropical structure to that of the semi-annual variations is suggestive of a modulation of the Hadley circulation as described by Newell et al. (1974) for the semi-annual case. Madden and Julian believed that the amplitude modulation of the motion was due to increased convection over the west pacific, and if measurements show this to be the case a related modulation of the Hadley cell flux could be expected.

Another question which still has to be resolved is the reason for the time scale of 40-50 days. As noted by Madden and Julian, the broadband nature of the time series would seem to rule out any tidal effects. A broadband peak such as this could result from either the stochastic forcing of a system with the bandwidth of the observed oscillation, or the response of a broadband system to forcing with preferential time scales. Webster (1973) examined the properties of the linear equatorial waves and concluded that the 40-50 day periodicity was probably the result of forcing with 40-50 day time scales. Experiments with the GFDL model (Hayashi 1973) also failed to show strong dynamical resonances at 40 to 50 days.

In conclusion, I believe that the resolution of these questions will probably require further measurements,

particularly in the area of the tropical forcing, especially air-sea interactions as suggested by Madden and Julian (1972), and calculations of the variations in northern hemisphere eddy transports. It seems that the well-defined northward phase propagation should assist in the study of the connection mechanisms and the understanding of this effect may aid greatly in the study of other tropical influences on the mid-latitudes.

APPENDIX A

As shown by Figure 4-1 a large step-like change occurs in the global M time series around day 240 (Sept. 1, 1976). Figures A-1 and A-2 show maps of the mean departure from the 1977-1980 climatological values for the months of July 1976 and October 1976 respectively. The maps show a large negative anomaly in the southern hemisphere high latitudes before the step. This feature appears as all heights and has a magnitude of greater than 7 M/S at the surface. These figures also show an equatorial response similar to the 45 day pattern which I believe is due to the atmospheric response to the 1976 El Nino as described by Selkirk (1982).

To test the reality of this change I have examined the monthly mean 500 mb winds from the high latitude southern hamisphere stations which are compiled in Monthly Climatic Data for the World (NOAA 1976). The four stations which are in the affected area are Marion Island (46S, 38W), Punta, Areans, Chile (53S, 71W), Comodoro Rivadavia Argentina (46S, 57W), and Invercargill, New Zealand (46W, 168E). Monthly mean data for 300 mb winds were also available which were also available which were compiled from the Australian Meteorological Research Center southern hemisphere analysis (Chiu, personal communication). The monthly mean zonal wind values from these sources are given in Table A-1. As mentioned before, the NMC analysis shows a positive step in September. The Australian analysis shows a negative

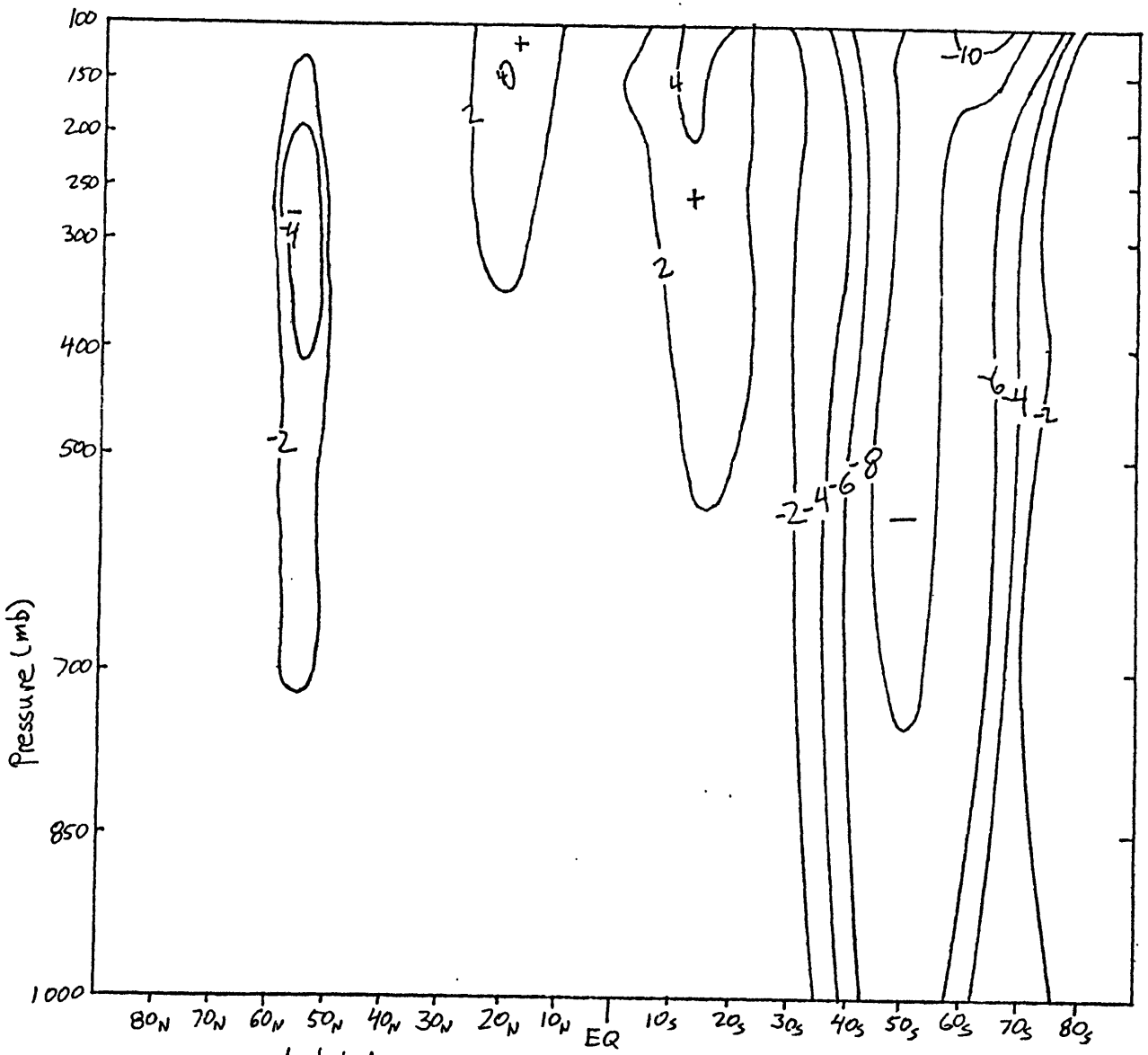

Fig. A-1. Mean [U] anomaly, July 1976

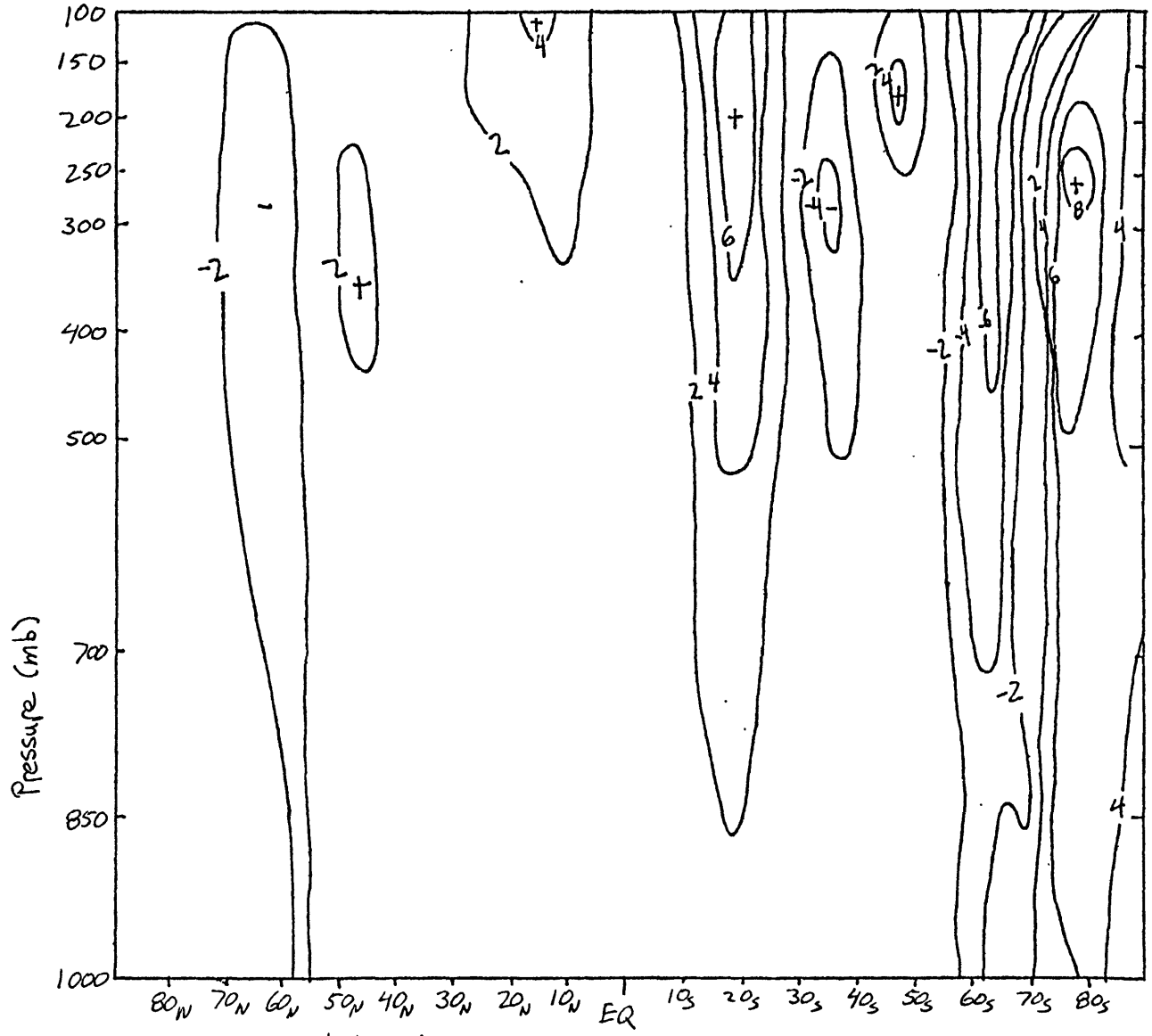

Fig. A-2. Mean [U] anomaly, October 1976

	[U] monthly means (m/sec)			
	July 1976	Aug. 1976	Sept. 1976	Oct. 1976
NMC 50°S 500 mb.	8.0	9.8	15.2	17.8
Aust. 50°S 300 mb.	23.6	22.5	20.2	22.3
Marion Island 46°S 500 mb.	23	25	19	25
Punta Arenas 53°S 500 mb.	17	17	12	7
Comodora Rivadavia 46°S 500 mb.	missing	15	12	10
Invercargill 46°S 500 mb.	13	3	24	9

Table A-1
Monthly Mean winds 45°S-50°S

step-like feature at this time. The station data does not show such dramatic changes, but tends to support the Australian values more than the NMC values.

In view of this uncertainty I have chosen not to use the NMC data for this area before the transition, thus the seasonal climatology consists of only 1977-1980 values.

APPENDIX B

The power spectrum of a weakly stationary process is generally defined as the Fourier transform of the autocorrelation function and is given by [B2] where the autocorrelation function is defined, for a real process, by [B1].

$$R_{xx}(\tau) = E[x(t)\,x(t+\tau)] \qquad [B1]$$

E[] is the expectation value operator.

$$P_{xx}(\omega) \propto \int_0^\infty R_{xx}(\tau)\cos\omega\tau\, d\tau \qquad [B2]$$

Using: $R_{xx}(\tau) = R_{xx}(-\tau)$ for a real process.

The Blackman-Tukey (1958) (B-T) estimate of the power spectrum is given by [B3] following the above definition and is a windowed Fourier transform of a sampled estimate of the autocorrelation function.

$$\hat{P}_{xx}(\omega) \propto \sum_{\tau=0}^{T} W(\tau)\,\hat{R}_{xx}(\tau)\cos\omega\tau \qquad [B3]$$

Where $W(\tau)$ is a window function to allow the use of a finite length autocorrelation estimate.

The window function which I have chosen to use is one found to be optimum for a criterion relating estimate variance and spectral resolution by Papoulis (1973) and given by [B4].

$$W(\tau) = \frac{1}{\pi}\left|\sin\frac{\pi\tau}{T}\right| + \left(1-\frac{\tau}{T}\right)\cos\frac{\pi\tau}{T} \quad ; 0 \le \tau < T \quad [B4]$$

An unbiased estimate of the autocorrelation function is given by [B5]. This estimate is generally not used because there is no assurance that its Fourier transform is non-negative. Instead the biased estimate given by [B6] which can be efficiently computed by fast Fourier transform techniques is often used.

$$\hat{R}_{xx}(\tau) = \frac{1}{N-\tau}\sum_{t=0}^{N-\tau-1} X(t)\,X(t+\tau) \quad ; 0 \le \tau < T \quad [B5]$$

Where N is the number of available observations.

$$\hat{R}_{xx}(\tau) = \frac{1}{N}\sum_{t=0}^{N-\tau-1} X(t)\,X(t+\tau) \quad ; 0 \le \tau < T \quad [B6]$$

One major advantage of the B-T estimator is that given suitable assumptions about the process, it is possible to derive confidence limits for the estimator. These are given by Chatfield (1980) and for the parameters used in this work (N=1536, T=128, Papoulis window) are about $\pm$1.6 dB for 95% confidence.

The Capon (1969) maximum likelihood method (MLM) estimate of $P_{xx}(\omega)$ is computed as the reciprocal of the total energy in an order M optimal filter centered at frequency ω. These filters are constructed so that they have unity gain at

ω and minimize the sum of the power from all the other frequencies for a signal with a known autocorrelation function. The power spectrum estimate yielded by this approach is shown by Capon to be given by [B7].

$$P_{xx}(\omega) \propto \frac{1}{S^H R_{xx}^{-1} S} \qquad [B7]$$

Where R_{xx} is the autocorrelation matrix of the process, S is a signal vector given by $S=e^{iwt}$ and S^H is the conjugate transpose of S.

To produce a meaningful spectrum estimate the autocorrelation matrix must be positive definite. This can be assured by using [B6] as the autocorrelation estimator.

A disadvantage of using the MLM and most other nonlinear spectral estimators is that no analytical expressions for the expected error of the estimates exist. However, it has been shown by Haykin and Kesler (1979) that the error of the maximum entropy method (MEM) and MLM estimates asymptotically approaches that of the B-T estimator for large N.

The MEM estimate, which was introduced by Burg (1967), is based on the concept of prediction filtering. Given a length T filter of the form shown in [B8] which is in some way optimal in predicting the value of the next sample based on the previous T samples, it is then possible to create what is known as a prediction error filter (PEF).

$$\hat{X}(t+1) = \sum_{k=0}^{T} h(k)\, x(t-k) \qquad [B8]$$

The PEF is T+1 points long and is given by (1,-h(k)). The output of the PEF is simply the difference between the predicted value of the next point and the actual value. Burg derived the MEM spectral estimate by extending the input series in such a way that the amount of information expressed by the series was minimized. The resulting spectral estimate is given by [B9].

$$\hat{P}_{xx}(\omega) = \frac{1}{\left|1+\sum_{k=1}^{T} h(k) e^{i\omega k}\right|^2} \qquad [B9]$$

A somewhat more intuitive way of looking at the MEM estimator is to consider the output of the PEF filter. If the prediction filter is a good one, the output of the PEF should contain very little information and will be in some sense 'white'. Thus the PEF is a filter which takes the original series as its input and outputs a 'whitened' one. The MEM estimate of the process power spectra is then the reciprocal of the PEF frequency response.

Various techniques have been proposed for the calculation of the prediction filter coefficients. The one which I have used is due to Marple (1980) and minimizes the squared prediction error when applied to the original series forwards and backwards. This particular method does not require an

estimate of the autocorrelation function and can actually be used to generate one.

Burg (1972) has shown that the MEM and MLM estimates of the power spectrum are related by [B10] when the same autocorrelation estimates are used.

$$\frac{1}{\hat{P}_{xx}\{\text{MLM order } M\}} = \sum_{l=1}^{M} \frac{1}{P_{xx}\{\text{MEM order } l\}} \qquad [B10]$$

This relationship shows the order M MLM spectrum to be a sort of average of the MEM spectra for orders 1 to M. This gives some insight into the ability of the MEM estimator to detect lines and the MLM estimator to do a better job of depicting broadband processes.

APPENDIX C

In order to investigate the phase propagation behavior of a phenomenon it is often useful to construct a series orthogonal to the original one with the same energy and a 90 phase shift. Such a series is generally referred to as a Hilbert transform of the original series. A good description of the role of the Hilbert transform and the construction of Hilbert transformers is given in Oppenheim and Schafer (1975). In this work I am generally concerned with the construction of an orthogonal realization of a Hilbert transform of a bandpass filtered time series. The required sampling interval to completely define a band limited process is called the Nyquist interval and is equal to 1/2 of the period corresponding to the process bandwidth. For the output of the 45-day filter used in this work the Nyquist interval is about 50 days. I have chosen to sample the series at 30-day intervals, somewhat faster than required, so as to put the peak of the frequency response near the center of a sampled frequency domain whose limits correspond to 30- and 60-day periods. This is done so that no signal power is aliased to zero frequency where the frequency response of any Hilbert transformer is zero. A Hilbert transform pair of time series, I(t), and Q(t) are created from 44 samples of the band pass filter output as shown in [C1].

$$I(t) = \frac{1}{2\pi \cdot 44}\left(\sum_{k=1}^{43} A_k \cos kwt + \sum_{k=1}^{43} \beta_k \sin kwt\right)$$
$$Q(t) = \frac{1}{2\pi \cdot 44}\left(\sum_{k=1}^{43} A_k \sin kwt + \sum_{k=1}^{43} \beta_k \cos kwt\right) \quad [C1]$$

Where A and B are given by [C2].

$$A_k = \sum_{t=0}^{43} f(t) \cos kwt \qquad [C2]$$

$$B_k = \sum_{t=0}^{43} f(t) \sin kwt$$

$$w = \frac{2\pi}{44} \text{ in [C2] and [C1]}$$

f(t) is the sampled time series.

I(t) and Q(t) are orthogonal as defined by [C3] due to the orthogonality of the integral period sines and cosines.

$$\sum_{t=0}^{43} I(t)Q(t) = 0 \qquad [C3]$$

Because of this orthogonality I and Q explain completely independent parts of the variance of any series and one can define a complex correlation coefficient given by [C4].

$$|r| = \left(r^2(I,X) + r^2(Q,X) \right)^{1/2} \qquad [C4]$$

$$\text{Phase}(r) = \text{Arg}\left(r(I,X) + i\, r(Q,X) \right)$$

Where r(I,X) and r(Q,X) are the correlation coefficients I vs. X and Q vs. X, respectively.

It is also useful to extend the EOF analysis to amplitude-phase eigenvectors. Specifically the EOF expansion now takes the form given by [C5].

$$\hat{[U]}_N(\varphi,p,t) = \sum_{n=1}^{N} [l(\varphi,p)I(t) + m(\varphi,p)Q(t)] \quad [C5]$$

Where l and m are the in-phase and out-of-phase amplitudes associated with a time series I and its Hilbert transform Q.

The squared error after the first EOF is given by [C6].

$$E^2 = \sum_t \sum_\varphi \sum_p [U(\varphi,p,t) - l(\varphi,p)I(t) - m(\varphi,p)Q(t)]^2 \quad [C6]$$

Expanding the product and dropping terms which equal zero due to the orthogonality of I and Q gives [C7].

$$E^2 = \Sigma\Sigma\Sigma [2U^2 - 2Ulm - 2Umq + l^2I^2 + m^2Q^2]$$

$$= \Sigma\Sigma\Sigma U^2 + \Sigma\Sigma\Sigma [(U-lI)^2 + (U-mQ)^2] \quad [C7]$$

Now taking the Hilbert transform of (U-mQ), which preserves the error, gives (H+mI) where H is the Hilbert transform of U and yields [C8].

$$E^2 = \Sigma\Sigma\Sigma U^2 + \Sigma\Sigma\Sigma [(U-lI)^2 + (H+mI)^2] \quad [C8]$$

The first term is a constant so optimization requires minimizing the second summation. This is a traditional EOF problem for a sample consisting of U and H giving EOF's which represent l and -m. The absolute phase of the solution

is arbitrary.

The same analysis can then be repeated after removing the explained variance from U and H. If one constructs the eigenvectors of the covariance matrix of the combined U and H field each eigenvector will be repeated with the same amplitude and a 90^{o} phase shift. Any choice of one of each pair gives an optimal solution to the original problem which was stated as [C5].

ACKNOWLEDGEMENTS

My financial support for this work was provided by MIT-Lincoln Laboratory under the Staff Associate program. The data set was prepared with support from the NASA Lageos project under contract NAS5-25870. The Department of Energy also provided assistance and supported very helpful related work which was performed at MIT by Professor Newell and his colleagues under contract DE-Aco2-76EV12195.

I thank Professor Newell and Dr. Richard Rosen of Atmospheric and Environmental Research of Cambridge Mass. for their comments, advice and assistance related to this work.

I thank Melvin Stone and James Evans of MIT-Lincoln Laboratory for their support and encouragement.

I also thank Liz Manzi for her excellent work typing the manuscript.

Finally, I would like to express my gratitude for the personal concern and support given me by the late David Karp of Lincoln Laboratory. His help was instrumental in the continuation of my academic studies.

REFERENCES

Arkin, P., 1981: "The relationship between interannual variability in the 200 mb tropical wind field and the southern oscillation," Ph.d. thesis, Univ. of Maryland.

Blackman, R.B. and J.W. Tukey, 1959: *The Measurement of Power Spectra from the Point of View of Communications Engineering.* New York: Dover.

Burg, J.P., 1967: "Maximum entropy spectral analysis," Proc. 37th Meeting of Society of Exploration Geophysicists.

_____, 1972: "The relationship between maximum entorpy and maximum likelihood spectra," Geophys., vol. 37, pp. 375-376.

Capon, J., 1969: "High-resolution frequency-wavenumber spectrum analysis," Proc. IEEE, Vol. 68, pp. 1352-1354.

Chang, C.-P., 1977: "Viscous Internal Gravity Waves and Low-Frequency Oscillations in the Tropics," J. Atmos. Sci., 34, pp. 901-910.

Chatfield, C., 1980: *The Analysis of Time Series: An Introduction.* London: Chapman and Hall.

Goodman, N.R., S. Katz, B. Kramer, and M. Kuo, 1961: "Frequency response from stationary noise," Technometrics, 3, pp. 245-268.

Hayashi, Y., 1973: "Spectral andlysis of tropical disturbances appearing in a GFDL general circulation model," J. Atmos. Sci., 31, pp. 180-218.

Haykin, S. and S. Kesler, 1979: *Nonlinear Methods of Spectral Analysis.* New York: Springer-Verlag.

Hide, R., N. Burch, L. Morrison, D. Shea, and A. White, 1980: "Atmospheric Angular Momentum Fluctions and Changes in the Length of Day," Nature, 285, pp. 114-117.

Jordan, T. and D. Anderson, 1974: "Earth structure from free oscillations and travel times," Geophysical Journal of the Royal Astronomical Soc., 36, pp. 411-459.

Kay, S. and S. Marple, Jr., 1981: "Spectrum analysis--a modern perspective," Proc. IEEE, 69, pp. 1350-1419.

Lambeck, K., 1980: "Changes in lenght-of-day and atmospheric curculation," Nature, 286, pp. 104-105.

Langley, R., R. King and I. Shapiro, 1981: "Earth Rotation from Lunar Laser Ranging," J. Geophys. Res., 86, pp. 11913-11918.

Lau, N.-C. and A.H. Oort, 1981: "A comparative Study of Observed Northern Hemisphere Circulation Statistics Based on GFDL and NMC Analyses. Part I: The time-mean fields," Mon. Wea. Rev., 109, pp. 1380-1402.

Lorenz, E., 1956: "Empirical orthogonal functions and statistical weather prediction," MIT Statistical Forcasting Project, Sci. Rept. No. 1.

Madden, R. and P. Julian, 1971: "Detection of a 40-50 day oscillation in the zonal wind in the tropical Pacific," J. Atmos. Sci., 28, pp. 702-708.

_____ and _____, 1972: "Description of global-scale circulation cells in the tropics with a 40-50 day period," J. Atmos. Sci., 29, pp. 1109-1123.

Marple, S., 1980: "A new autoregressive spectrum analysis algorithm," IEEE Trans. Acoust., Speach, Signal Process., ASSP-28, pp. 441-454.

Newell, R., J. Kidson, D. Vincent, and G. Boer, 1972: *The General Circulation of the Tropical Atmosphere, Volume 1.* Cambridge, Mass.: The MIT Press.

_____, _____, _____, and _____, 1974: *The General Circulation of the Tropical Atmosphere, Volume 2.* Cambridge, Mass.: The MIT Press.

NOAA, 1976: *Monthly Climatic Data of the World.*

Oppenheim, A. And R. Schafer, 1975: *Digital Signal Processing.* Englewood Cliffs, J.J.: Prentice-Hall.

Papoulis, A., 1973: "Minimum-bias window for high resolution spectral estimates," IEEE Trans. Inform. Theory, IT-19, pp. 9-12.

Rasmussen, E., P. Arkin, W.-Y. Chen and J. Jalickee, 1981: "Biennial variations in surface temperature over the United States as revealed by singular decomposition," Mon. Wea. Rev., 109, pp. 587-598.

Rosen, R. and D. Salstein, 1980: "A comparison between circulation statistics computed from convential data and NMC Hough analyses," Mon. Wea. Rev., 108, pp. 1226-1247.

_____ and _____, 1981" "Variations in atmospheric angular momentum," Tech. Report A345-T1, Env. Res. and Tech., Concord, Mass.

Selkirk, H. 1982: "Seasonally stratified correlations of upper tropospheric winds to the Southern Oscillation," to be submitted to J. Climat.

Stacey, F., 1981: "Variability of the Earth's rotation," Nature, 289, p. 750.

Starr, V., J. Peixoto, and N. Gaut, 1970: "Momentum and zonal kinetic energy balance of the atmosphere from five years of hemispheric data," Tellus, 22, pp. 251-274.

Stevens, D. and G. White, 1979: Comments on "Viscous internal gravity waves and low-frequency oscillations in the tropics," J. Atmos. Sci., 36, pp. 545-546.

Webster, P., 1973: "Temporal variation of low-latitude zonal circulations," Mon. Wea. Rev., 101, pp. 803-816.